Marius Volmer

Sensors and microsensors

Theoretical and practical notes

EDITURA
UNIVERSITĂȚII
TRANSILVANIA
DIN BRAȘOV

2022

ISBN 978-606-19-1576-7

Table of Contents

Preface

In a broader definition, a sensor is a device that receives a stimulus and responds with an electrical signal. The human eyes are complex light sensors that transmit electrical signals received and decoded by our brains. Our skin is a high sensitivity pressure and temperature detector. The brain of the bird contains a complex magnetic sensor that is used as a navigation tool. Many other examples can be found in nature.

Sensors are used in everyday objects such as mobile phones, the room thermostat, touch-sensitive elevator buttons and so on. Modern cars contain a large number of sensors used to control the engine operation, cabin temperature or for safe navigation. A modern sensor does not function by itself; it is always a part of a larger system that sometimes may incorporate other detectors, signal conditioners, signal processors, and various analog and/or digital interfaces. Microsensors are two- and three-dimensional micromachined structures obtained by using the integrated circuit technology (IC). They have smaller size, improved performance, and can be found in monolithic or hybrid ICs which can deliver analog and/or digital signals. The relatively large output signal simplicity of connection with other electronic circuits makes them very attractive for sensing applications.

However, there are many applications that require using sensors "as they are" which do not contain other functional blocks like amplifiers, digital to analog convertors and so on. This approach offers the flexibility to build custom applications and to develop special sensing techniques. For example, in cryogenic devices are used semiconductive temperature sensors, as Cernox, which are thin film resistors with negative temperature coefficient. At such low temperatures the sensors cannot accommodate on the same chip the electronics used for signal conditioning and interfacing with other circuits. Sometimes, at these low temperatures, the sensors can be subject, also, to very large magnetic fields that can introduce perturbations in electronic circuits. This is the case of Nuclear Magnetic Resonance equipment used for medical diagnosis.

This book presents fundamentals on different types of sensors, the physics that govern their functioning, specific characterization techniques and basic applications. Also are presented typical circuits used for sensors excitation, signal conditioning, data acquisition and graphical representation in order to get useful information for the device under test. In this book are presented: temperature sensors, force sensors, light sensors, magnetic field (Hall and magnetoresistive) sensors and current sensors. Because is discussed a new type of sensors, based on giant/tunneling magnetoresistance effect, are presented two freeware simulators, Simulmag and OOMMF, that are useful for device designing and studies on how these structures behave in magnetic field. For graphical representations, the reader will learn to use another free application, SciDAVis, for **S**cientific **D**ata **A**nalysis and **Vis**ualization, that is very similar with other commercial products.

The content of this book is especially aimed at students from Electrical Engineering and Computing study program that are attending the course on "Microsensors and Actuators" but can be useful for any students or engineers that are working in the field of sensors and measurement equipment. Basic knowledge of analog and digital electronics, physics and electromagnetic field theory is required.

This work was supported by a grant of the Ministry of Research, Innovation and Digitization, CCCDI - UEFISCDI, project number PN-III-P2-2.1-PED-2021-3112, 597PED/2022, within PNCDI III

I. Computer simulation of magnetization curves in magnetic thin films with Simulmag

1. Introduction

Currently there is much interest in the transport and magnetic properties of metallic multilayer systems since the discovery of the giant magnetoresistance (GMR). Usually, the magnetic properties of the thin films are investigated using a Vibrating Sample Magnetometer (VSM) or other methods like Kerr magnetometry. In this practical work we use a micromagnetic simulator based on Stonner-Wolfarth model to investigate the hysteresis loop of $Ni_{80}Fe_{20}$ (Py) thin films and Py/Cu/Py multilayers. The program, SimulMag (developed at NIST by Dr John Oti), calculates the interaction between the single-domains elements and the applied magnetic field. The element's magnetic properties, such as magnetization, anisotropy, pinning fields, must be specified or selected from a library of materials. The careful choice of the dimensions, the configurations and properties of elements permits the modeling of a wide range of technologically interesting systems.

2. Theoretical aspects

In this approach the basic design unit is an *element* shaped as a rectangular prism. The element is oriented parallel to the coordinate axes of the system, Fig. 1. The element may be *ferromagnetic* or *nonmagnetic*.

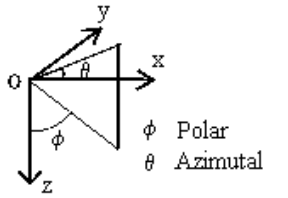

Fig. 1. Description of the coordinate system used by this simulator

The ferromagnetic element is a *single-domain element*, which means that it is uniformly magnetized and can thus be characterized by a single three-dimensional magnetization vector. The magnetization vector is free to rotate in three dimensions under the influence of magnetic fields. The properties of the elements and the interactions between them are specified by the user. To obtain the response of the system is used the energy minimization calculation in which an energy minimum is calculated for the system for a given value of applied magnetic fields. The equilibrium magnetization states of elements for static calculations are those that yield a minimum of the total free energy density of the system $E = \sum_i e_i$, where e_i is the free energy density of the element given by the expression:

$$e_i = \frac{1}{2}\vec{M}\cdot\overline{\mathbf{N}}\vec{M} - \vec{H}_{\mathbf{T}}\cdot\vec{M} \qquad (1)$$

where the self-demagnetization tensor $\overline{N}$ is expressed by a diagonal matrix whose nonzero elements (N_x, N_y, N_z ; $N_x + N_y + N_z = 1$ in S.I.) are the demagnetizing factors of a uniformly magnetized ellipsoid with the same aspect ratio and principal axes (x, y, z) as the element.

$$\overline{N} = \begin{pmatrix} N_x & 0 & 0 \\ 0 & N_y & 0 \\ 0 & 0 & N_z \end{pmatrix} \qquad (2)$$

Such an ellipsoid is called an *equivalent ellipsoid* of the element. $\vec{M}$ is the magnetization vector of the element and $\vec{H}_T$ is the total effective field from all other sources excluding self-demagnetization. The first term on the right side of (1) represents the self -demagnetization energy of the element and the second term, the energy due to other magnetic interactions. The self-demagnetizing field sources for a uniformly magnetized element are the magnetic *surface charges* formed on its bounding faces. For a system composed of several elements, the field $\vec{H}_T$ is a function of the magnetization of all elements of the system. This necessitates the use of self-

consistent iterative methods in obtaining an energy minimum for the system. During iteration, the magnetic moments of the elements are rotated in a manner that minimizes their local free energy densities given by (1). This is accomplished by using a numerical implementation of the classical Stoner-Wohlfarth model that is applicable to general single-domain ellipsoids. This method finds the equilibrium magnetization orientation of an element. The updated magnetization values are used to recompute $\vec{H}_T$ for each element, and this iteration procedure is repeated until the magnetization of the system reaches equilibrium. The calculation stops when "The convergence tolerance" criterion, from the "Calculation Preferences" tab, is reached. The default value is 1 degree.

In the case of thin films, we must consider a thin rectangular prism that lies in the xy plane. For thin films $N_Z \approx 1$. This high value of the demagnetizing factor produces a shape anisotropy. For example, if we consider a 10x10 μm^2 and 100 nm thick single-domain Permalloy thin film the self-demagnetization tensor becomes (N_x, N_y, N_z)=(0.017, 0.017, 0.966). The self-demagnetizing field under z direction (the shape anisotropy) is H_D=760 kA/m, i.e. H_D=9600 Oe. Because it is most suggestive in what follows we will use CGS units (see the Annex 1). On the other hand, the film may present an easy direction of magnetization defined by the direction of the anisotropy field, H_K. Usually, for Permalloy, H_K=5 Oe. We present, in Fig. 2, the results of simulations made for a 10x10 μm^2 single-domain Permalloy thin film.

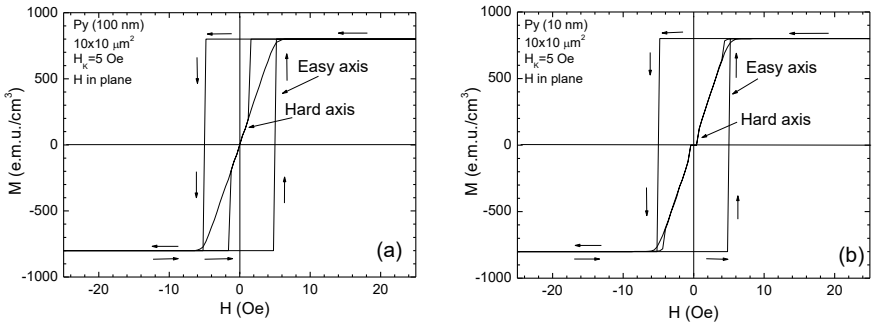

Fig. 2. Simulation of M-H hysteresis loops for a 100 nm (a) and 10 nm (b) single-domain Permalloy thin film. The arrows are guides for the eyes.

From Fig. 2(a) we can see the importance of the demagnetizing fields in the film plane which produce a split of the M-H hysteresis loop under the hard axis. For a 10 nm thin film the demagnetizing coefficients are (N_x, N_y, N_z)=($1.84 \cdot 10^{-3}$, $1.84 \cdot 10^{-3}$, 0.998) which lowers the demagnetizing fields in the film plane but enhances the demagnetizing field on a direction normal to the film plane. However, the thin film may have a complicated spin structure, not a single domain structure, in a way to reduce the dominant magnetostatic interactions. One example of the complicated spin structure is the magnetization curling formed at the edge of the layers. For this reason, must be used a more realistic structure consisting in a large number of single-domains which interact between them and with the applied magnetic field.

Sometimes, the magnetic multilayers like Permalloy/Cu/Permalloy exhibit a ferromagnetic interlayer coupling. It was shown that the dependence of the coupling constant J on the Cu-layer thickness, for t_{Cu}>1.5-2 nm, is well described by the Néel model for magnetostatic interlayer coupling, based on the interaction between the dipole fields produced by rough interfaces:

$$J = \frac{\pi^2}{\sqrt{2}} \frac{h^2}{\lambda} \mu_0 M_S^2 \exp\left(\frac{-2\pi\sqrt{2} t_{Cu}}{\lambda} \right) \qquad (3)$$

Here, λ and h are the lateral length scale and amplitude of the roughness, respectively, and M_S is the saturation magnetization (M_S=800 kA/m or 800 emu/cm^3 in CGS). In this model the roughness is assumed to be two-dimensional and sinusoidal. Here, λ is determined by the grain size. These parameters can be obtained from AFM measurements; some typical values are h=1.35 nm and λ=15 nm. If we consider t_{Cu}=4 nm the interlayer coupling is J=0.23 mJ/m^2. For this value the coupling field is H_0=2457 A/m (31 Oe). This value is correct only if we consider the magnetic layers completely separated by the Cu spacer. Because of Permalloy bridges that exist trough the spacer, the coupling may have local variations that exceed 31 Oe.

3. Specific simulations to be performed by students

a) The **SimulMag** program can be downloaded (http://math.nist.gov/oommf/contrib/simulmag/), installed. and launched. A copy of this installer is on the CD as well. Some compatibility settings may be applied before the installation. The following main window will be displayed when the program is launched, Fig. 3:

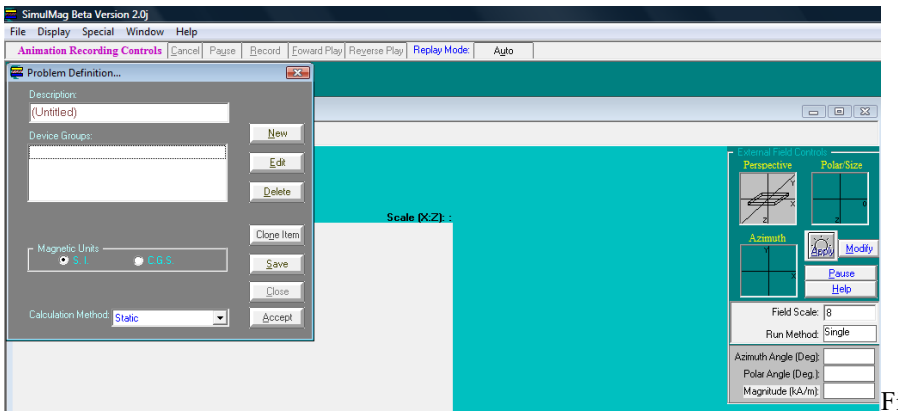

Fig. 3

b) The design steps will be followed using the interactive menu and the guidance provided by the instructor. Some steps are illustrated bellow, Fig. 4:

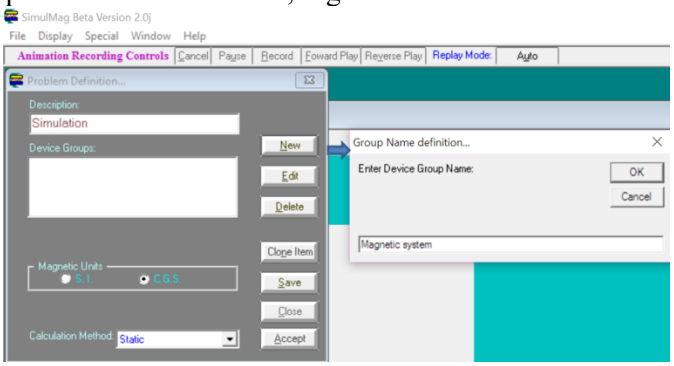

Fig. 4

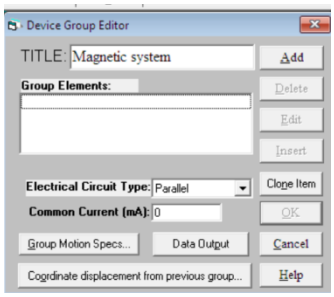

Write a title in "Description" window then press "New" and give a name for the "Device Group" like "Magnetic system". Finally, press "OK". A new window "Device Group Editor" will be displayed. Here you can add **elements** by pressing "Add".

c) **A simple structure** 1000x1000x10 nm^3 from Permalloy will be designed by filling up with data in the "Media Characteristics" window; a uniaxial anisotropy field H_K=20 Oe over x axis will be considered (see Fig. 1 and Fig. 5);

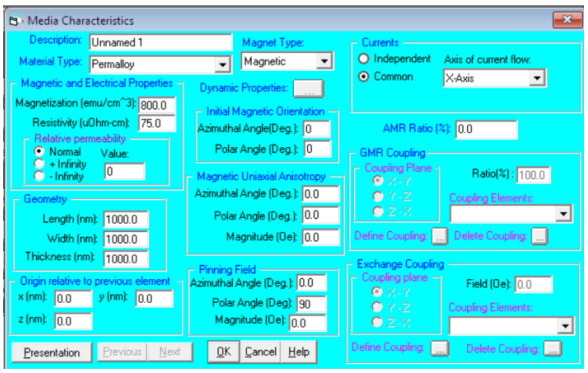

Fig. 5

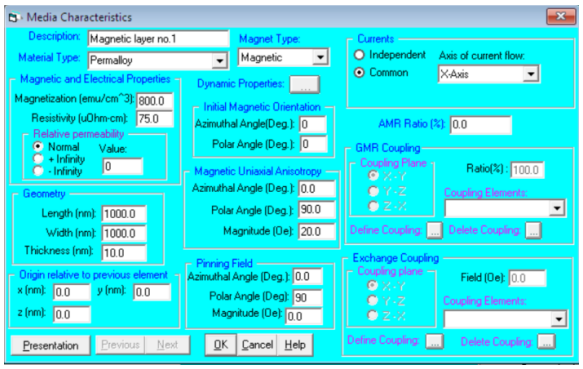

Press OK. Press "Data Output" to select "Magnetization along field vs. External Field" to be displayed.

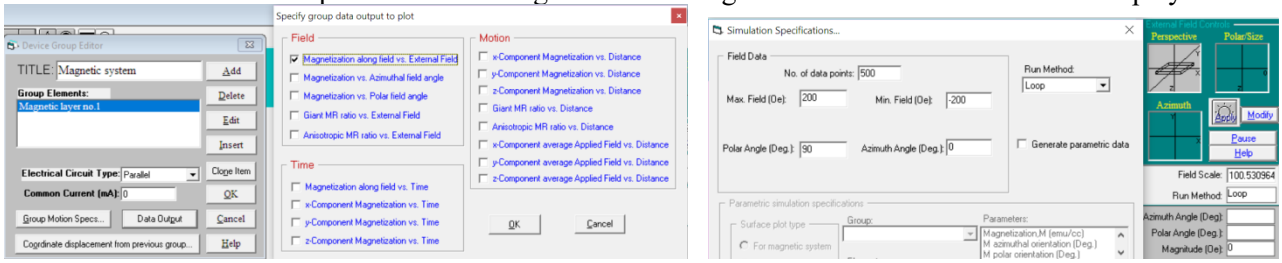

Fig. 6

d) M(H) will be plotted for different orientations of the applied field. To do this, select "Modify" then chose "Loop" in "Run Method". Select a number of data points and the interval for the applied field. If you select

500 data points, they will be distributed uniformly in this range as follows: 200 Oe →0→-200→0→ 200 Oe (in order to define a magnetization cycle). So, data will be displayed for each 16 Oe. Chose 90 for the Polar angle and 0 for Azimuthal angle (see Fig. 1) then run the simulation. Chose 90 degrees both for Polar and Azimuthal angles and run again the simulation. Observe the main difference. Data can be saved by making right-click on plot.

e) **A multilayer system** will be designed. The structure consists from two 1000x1000x10 nm^3 Permalloy layers separated by 30 nm interlayer (usually from Cu). The anisotropy field H_K=20 Oe over x axis will be considered for both layers. A positive exchange coupling field H_{coupl}=80 Oe between the magnetic layers will be considered. The magnetization from the second magnetic layer will be pinned with a pinning field H_{pin}=200 Oe. A GMR coupling will be considered, also for this system. The amplitude for this coupling will have an arbitrary value (ex. 10%). For real structures, this amplitude depends on the layers properties.

f) Easy axis and hard axis M(H) and GMR(H) simulations will be run for small (±100 Oe) and medium fields (±300 Oe).

g) **A MRAM memory cell**, which is using this ML structure, will be designed; a file with the design parameters will be provided. As cell memory will be used the structure defined at section e). The bit and word lines have 10000 nm x 1000 nm x 100 nm (thickness). The cell memory is "Group 0", the "Bit line" is Group 1 and the "Word line" is Group 2. See below.

4. Some examples of "how it should appear the simulations"

4.1. Results for section d: Permalloy thin film 1000x1000x10 nm^3

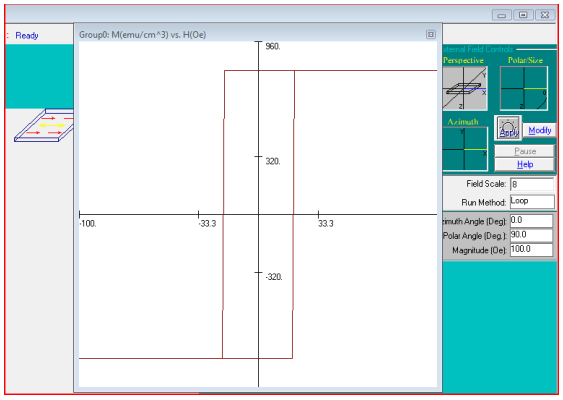

Fig. 7. H is applied over the easy axis

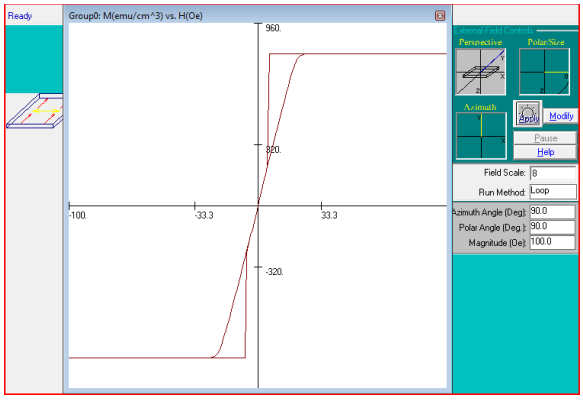

Fig. 8. H is applied over the hard axis

4.2. Results for sections e-f: Permalloy(10nm)/Cu(30 nm)/Permalloy(10 nm)/AF layer (for exchange biasing pinning field)

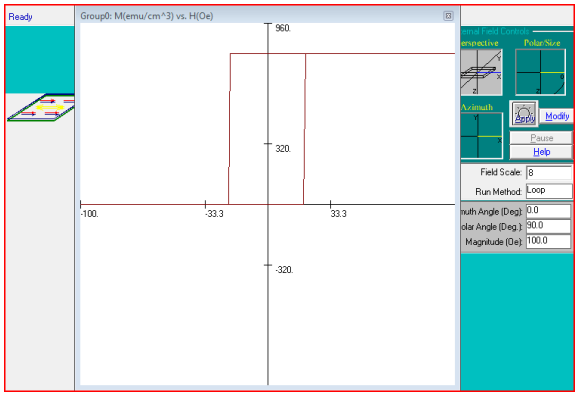

Fig. 9. Easy axis low field magnetization curve

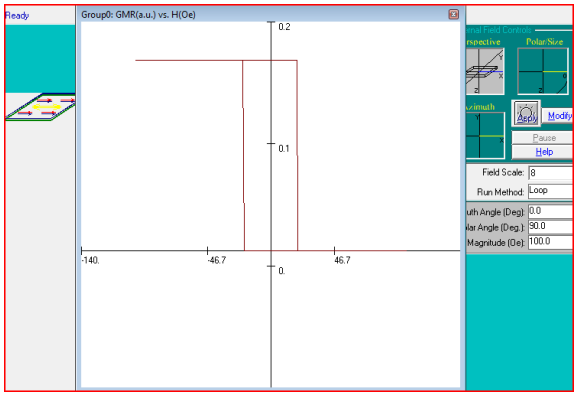

Fig. 10. Easy axis low field GMR(H) curve

For this regime, named low field, only the "free layer" can switch his magnetization. Such behaviour is used for magnetic memories and read heads applications.

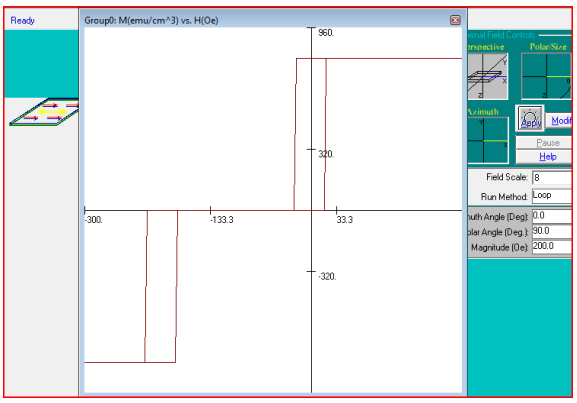

Fig. 11. Easy axis, large field, M(H) curve

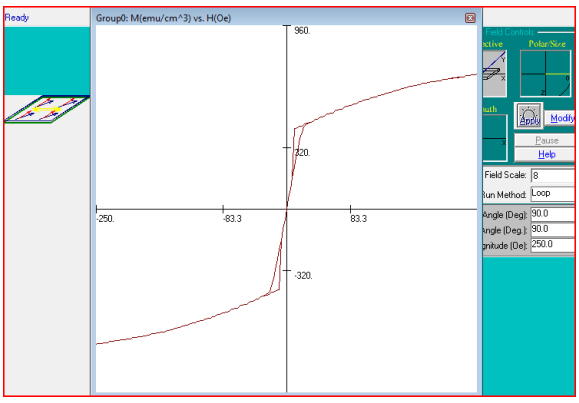

Fig. 12. Hard axis, large field, M(H) curve

Note that when H is applied over easy axis, for large enough fields, the pinned layer can switch his magnetization as well, at –200 Oe, Fig. 11, which is the amplitude of the pinning field. The width of the hysteresis curves, both for free and pinned layers, is decided by H_K=20 Oe. For hard axis magnetization curve the hysteretic effect is very low which is beneficial for sensing applications.

4.3. Results for section g: simulations of a MRAM cell

The following structure should be designed (as in the example file):

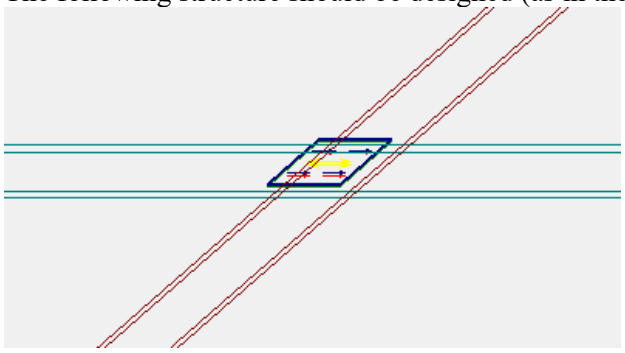

Fig. 13. MRAM cell basic schematics – initially, both layers have parallel orientations of the magnetic moments: R_{memory} = low – 0 logic

Each metallic stripe placed beneath the MRAM cell has 10000 nm x 1000 nm x 100 nm (thickness).
The MRAM cell is a GMR element used for simulations at sections e-f
a) A current of 2 mA will be set trough the horizontal stripe (bit line), Fig. 14.

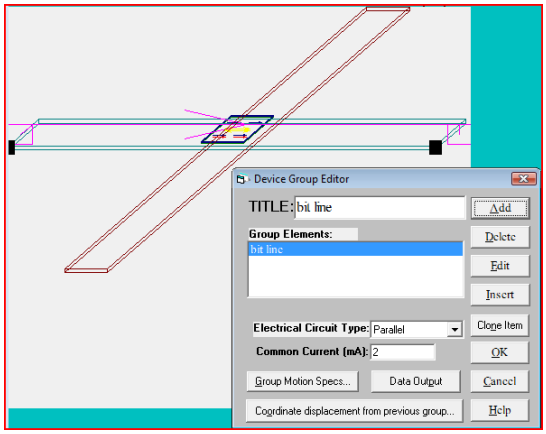

Fig. 14. Initial magnetic state

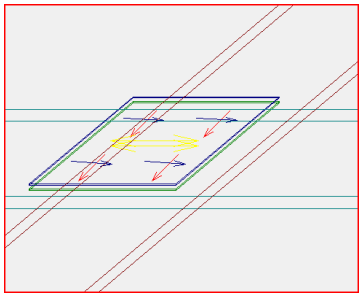

Fig. 15. The magnetic state for I=2 mA in “bit line”

The following spin configurations, Fig. 15, in free and pinned layers will be obtained by micromagnetic simulation.
Set again the current to 0 and see what is happening after the simulation is run again. The magnetic moments should return to their initial orientations i.e., the information was not stored.

b) Having, simultaneously, 2 mA in the bit line and -2 mA in the word line (opposite to y axis) and running the simulations the following state should be reached, Fig. 16. When both currents will be set to 0, the simulation has to give a *new stable state*, like in Fig. 17, with antiparallel orientations of the magnetic moments. The information was written and stored. The magnetic moments have antiparallel orientations which means a larger electrical resistance of the structure that can be assimilated with a new logical state: R_{memory} = high – 1 logical state. This is the working principle of the MRAM which is a nonvolatile memory.

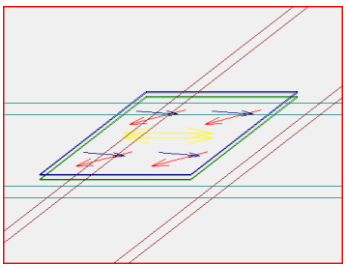

Fig. 16.

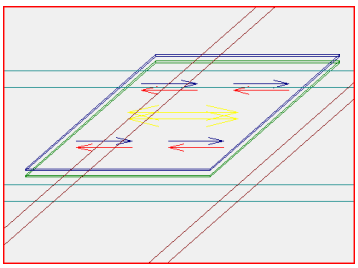

Fig. 17

Using a similar procedure, re-write in the memory cell the old state (parallel orientations of the magnetic moments): R_{memory} = low – 0 logic

Supplementary task: simulate a rotation sensor based on GMR effect (we must apply a rotating magnetic field in the film plane).
Useful tips: use the structure defined in section 3e). Then, select as run method "Rotation" and chose to perform 2 full rotations (for 720 data points) of the magnetic field in the film plane: H=100 Oe, Polar angle 0→720, Azimuthal angle 90. To display the simulation results check the fields like below. You should obtain (after data post processing) the plots illustrated bellow for M(angle) and GMR(angle). The curve GMR(angle) represents the output of a GMR rotation sensor.

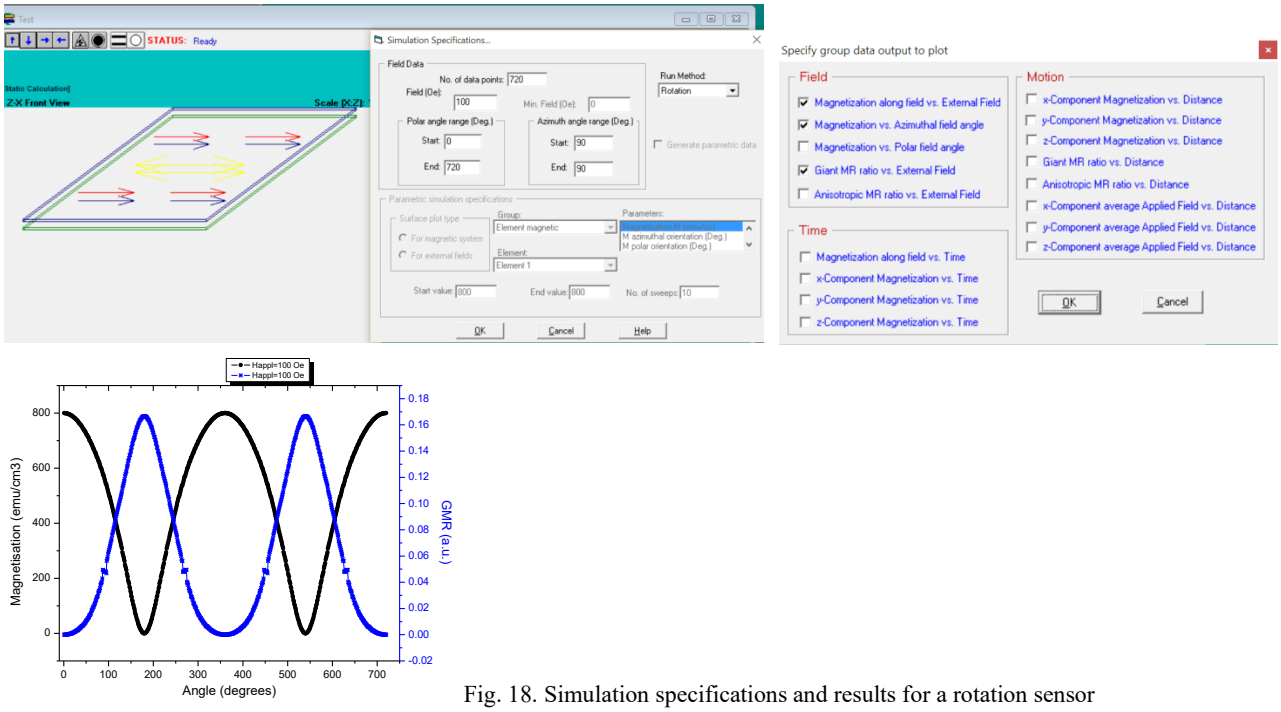

Fig. 18. Simulation specifications and results for a rotation sensor

4.4. Example of data processing

Data obtained from simulations can be plotted using different dedicated software solutions like Origin (commercial), Matlab, SciDAVis, Gnuplot, etc. The last two are freeware programs. In what follows, will be presented some steps to be followed using SciDAVis (https://sourceforge.net/projects/scidavis/) to plot data from Simulmag which exports data as .dat files.
As an example, will be used results obtained in Section 4.2.

To avoid some errors when importing data in SciDAVis, the file will be first opened with a simple text editor, like Notepad. Consider the file "magnetic_multilayer_M_easy_axis.dat", Fig. 19. Note that columns are reversed: first column represents the output, Magnetization, which *should be considered as y column* and the second column represents the applied field, H, which *should be considered as x column*. Delete the first line "Output :Group0: M(emu/cm^3) vs. H(Oe)" and save the file with other name in order to preserve the original one, Fig. 19. This approach must be considered for all the results exported from Simulmag.

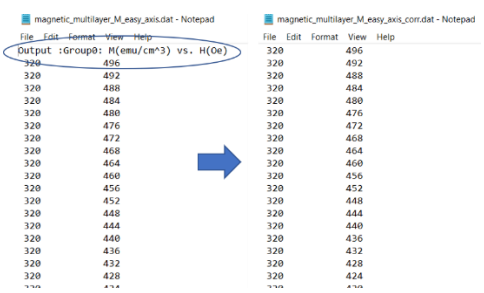

Fig. 19

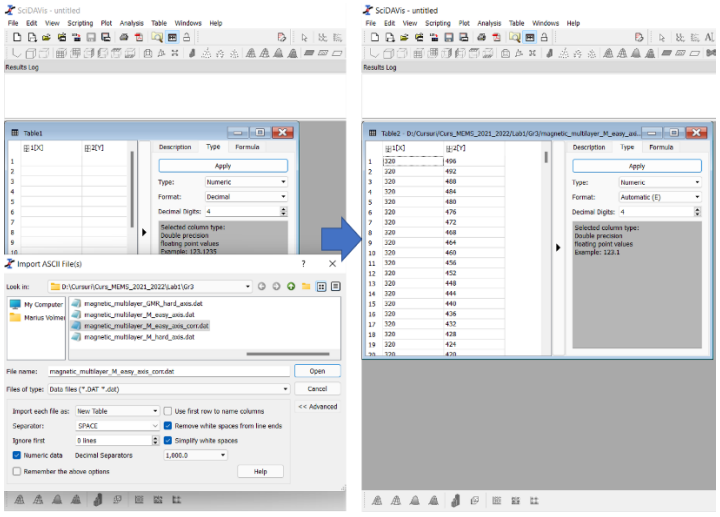

Fig. 20

Launch SciDAVis and from the main menu chose File → Import ASCII file(s). Select the file, use the settings from Fig. 20 then, click Open. Data will be imported like in Fig. 20. The steps described in Fig. 19, can be avoided if we chose to "Ignore first" 1 line (see Fig. 20), i.e., to ignore the description line from the data table, Fig. 19. Please note that first column represents the simulation output (Magnetization in this example) and the second column represents the input, e.g., the applied field, in this example. So, the role as x and y columns must be switched. The following steps must be followed, Fig. 21: (i) select first column, chose the tab "Description" and write the name of this column (M (emu/cc)) and in the "Comments" field you can introduce a text like "Magnetization along the easy axis". To validate your changes, you must click "Apply". Following the same you can name the second column as H(Oe), Fig. 21. To declare the role of each column, make right click on the column header M (emu/cc), chose "Set column as" and select "y". Now, this will be assigned as a y column. Following the same steps, you can assign the column H(Oe) as x column.

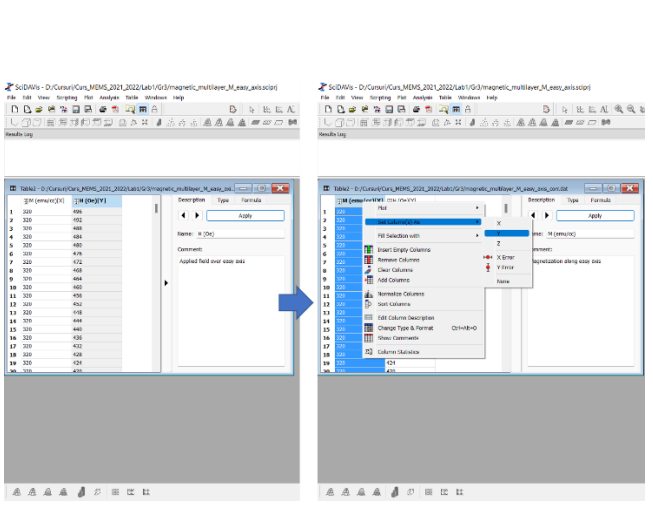

Fig. 21. Setting the columns and their roles (x,y)

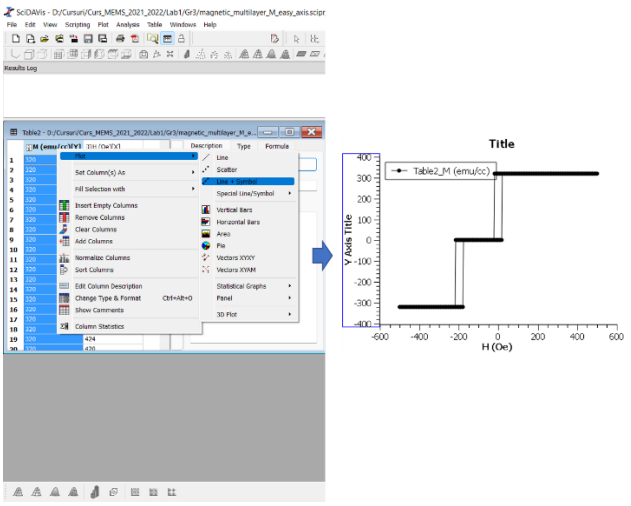

Fig. 22. Plotting M(H)

To plot magnetization in function of the applied field, select column M(emu/cc) and chose Plot (both from the main menu or using the shortcut: right click – Plot); select "line+symbol". We must note that at about -200 Oe, the pinned layer switches his magnetization; see also Fig. 11. Edit the plot by labelling x and y axes and specifying a "Title". The plot can be exported as a graphical image by choosing File and "Export Graph" or by copying the selected image with Ctrl+C. You can try many other refinements on this plot.

II. Using Object Oriented Micromagnetic Framework (OOMMF) computer program to simulate magnetization curves in magnetic thin films

1. Introduction

Magnetization dynamics in thin films based micro- nanometre scale structures is a crucial in the development of novel technologies and applications including sensors, various types of magnetic memories, etc. On the same time, we must note that some properties like magnetoresistance effect (MR), Anisotropic magnetoresistance effect (AMR), Hall effect or Planar Hall effect (PHE) depend on the magnetic behaviour of the structure. Usually, the magnetic properties of the thin films are investigated using a Vibrating Sample Magnetometer (VSM) or other methods like Kerr magnetometry.
On the other hand, the magnetic properties can be simulated. Comparing experimental results with simulations represents a powerful tool used in analysis and designing process of micrometer sized magnetic devices. In this practical work the student is familiarized with a micromagnetic simulator based on "Object Oriented Micromagnetic Framework" (OOMMF) computer program, developed at NIST https://math.nist.gov/oommf/.
The careful choice of the dimensions, the configurations and properties of elements permits the modeling of a wide range of technologically interesting systems.

2. Theoretical aspects

OOMMF is based on the solution of the Landau-Lifshitz-Gilbert (LLG) equations as applied to *finite elements* into which the material to be simulated is divided. OOMMF discretizes the sample using a grid of cubic cells of a size given by the user and considers a uniform magnetization inside each cell. This process can be done automatically for virtually any shape provided by the user. Usually, the cell size should be smaller than 10 nm (on each side) to get accurate results. This size depends on the material nature and is related with the so called "characteristic length" which can define the maximum cell size inside of which there is a uniform magnetization. This cell behaves like a single domain region.
The equilibrium magnetization configuration results from the minimization of the system's free energy which is subject, or not, to an applied external magnetic field. The energy of a ferromagnetic system composed from these cells (as modeled in the software) is composed of: the mean field exchange energy E_{ex} between nearest neighbors characterized by the exchange coupling constant A (J/m); the magnetocrystalline anisotropy energy, which describes the interaction of the magnetic moments with the crystal field characterized by the constant K_1 (j/m^3); the damping parameter α is not well known. Values of α between 0.005 and 2.0 have been used to solve LLG. The damping parameter was not found to change the equilibrium magnetization configurations in uniform ferromagnetic systems. More about solving the LLG equation can be found on https://math.nist.gov/oommf/.

3. Specific steps to be followed to run a simulation

a) The program can be downloaded from https://math.nist.gov/oommf/software.html. It should be used the latest beta version, not alpha version which represents a development version. For Windows users it can be used a 32- or 64-bit pre-compiled version. An installation kit can be found on the accompanying CD.
b) Launching the program and preparing a simulation.
When launching the program, the following main window will be displayed:

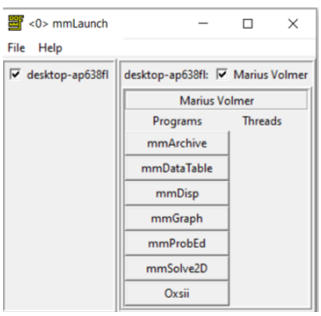

Fig. 1. *OOMMF, starting window*

Before to start to design and simulate a structure, it is preferable to open the useful windows like in Fig. 2.

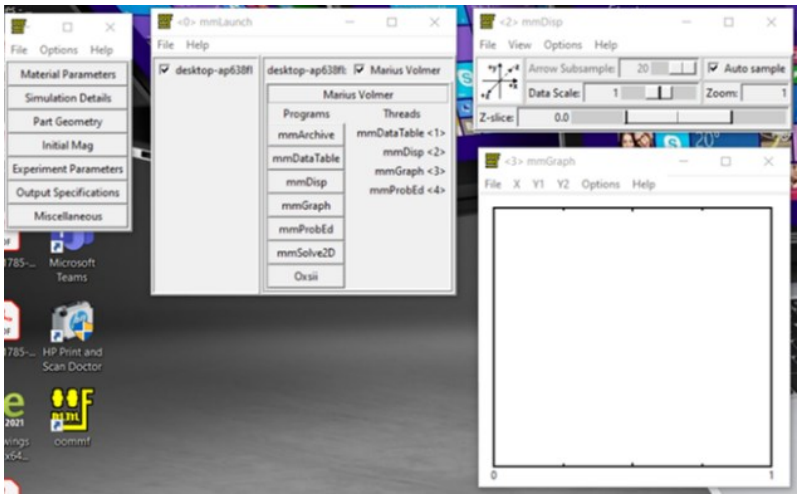

Fig. 2. Useful windows that need to be opened before you can to start designing and simulating a magnetic structure

This gives a menu of options like: mmArchive (to auto-save scalar and vector field data), mmDataTable (to display current values of scalar outputs), mmDisp (to display vector fields), mmGraph (to plot x-y graphs), mmProbEd, to view, edit or modify a 2D problem (layers with a given thickness) and 2D solver mmSolve2D where the results can be visualized in different z-slices. Oxsii controls the 3D solver but the problem can be defined only using a text editor. Many examples are present and can be adapted to specific needs A detailed description of each library as well as a quick setup guide is given in the OOMMF user guide. Note that many tutorials are available on the internet.

The graphical interface of the software allows the setting of the main parameters of the LLG equation as well as the physical dimensions of the mask to be simulated (Fig. 3 shows necessary tabs to configure astructure for a simulation). You can import a 2D image (**only <u>black-white</u>**) or use a predefiend shape as shown below. The black regions will be interpreted by the simulator to represent magnetic material whereas the white regions represent nonmagnetic material (vacuum from the point of view of simulator).

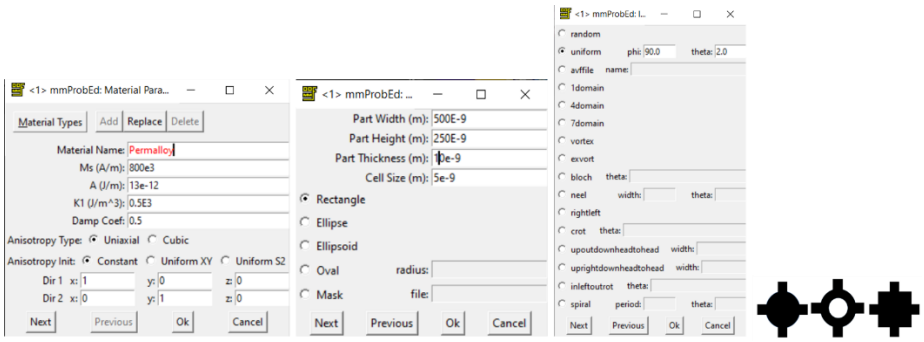

Fig. 3. mmProbEd most important tabs: Material Parameters, Part Geometry and Initial magnetization tabs; also, are illustrated 3 images that can be imported to define a specific layout.

The material employed for simulation in this example is named Permalloy ($Ni_{80}Fe_{20}$) widely used to build magnetic sensors. The material parameters like saturation magnetization, M_S, exchange coupling constant, A, and uniaxial anisotropy constant, K1, can be set by the user. The simulated structure is a rectangular plate of 500x250x10 nm^3, see Fig. 3, which is divided into cubic cells of 5 nm each side. Initial magnetization is set in film plane, along x axis with a small deviation of 2 degrees (this has a physical meaning, i.e., magnetization lies in the film plane and the small misalignment is useful to give for solver the initial conditions to find the magnetic moments orientations for each applied value of the magnetic field).

The tab “Experiment Parameters” from “mmProbEd” allows user to set the virtual experiment when magnetic field is applied to sample (x, y, z directions). To record a full hysteresis loop over x axis the following settings can be applied, Fig. 4.

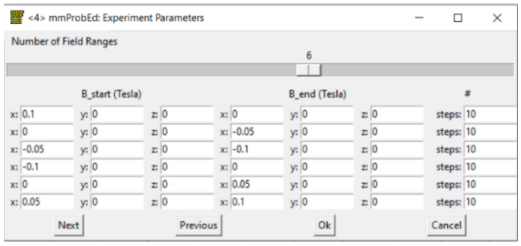

Fig. 4. The field is applied over x axis; the field ranges and number of steps are specified by the user

4. Some examples of "how it should appear the simulations"

Results for: 500x250x10 nm^3 Permalloy film; the cell is 5 nm each side

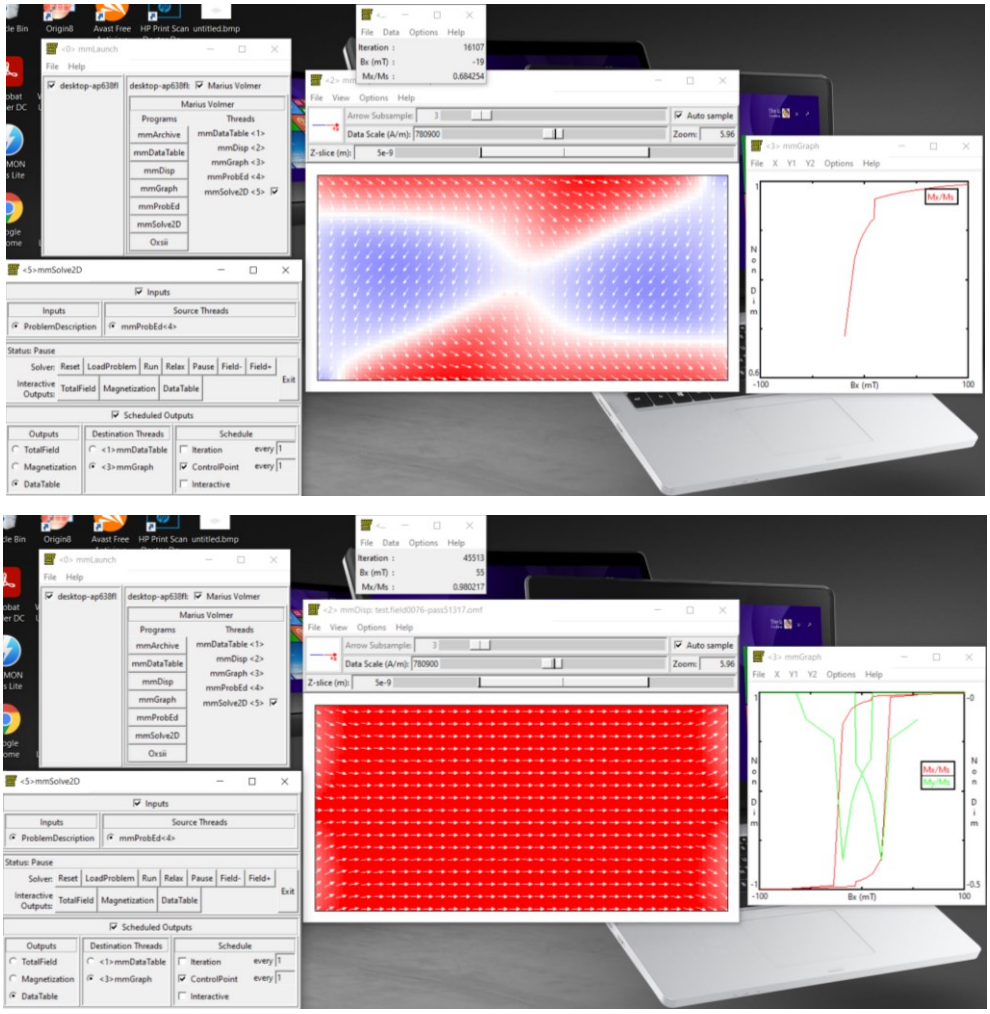

Fig. 5. Images taken for two fields during the simulations and some settings to be applied

To save data for magnetization curves you must select in window mmGraph the tab File → Save As... Then make the appropriate selections like in Fig. 6.

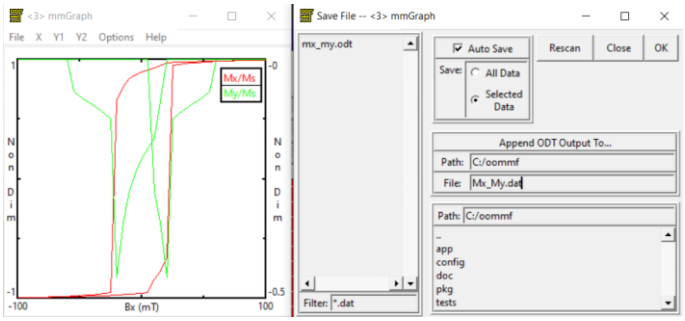

Fig. 6. Saving data for M_x and M_y in function of the applied field, B_x.

To represent these dependencies with SciDAVis it is advised to open the .dat file with a simple text editor, like Notepad, delete the text information, see Fig. 7, and save the file with a new name. To import data in SciDAVis you must use the settings described in Fig. 7. The Mx_My.dat file used as example can be found on CD.

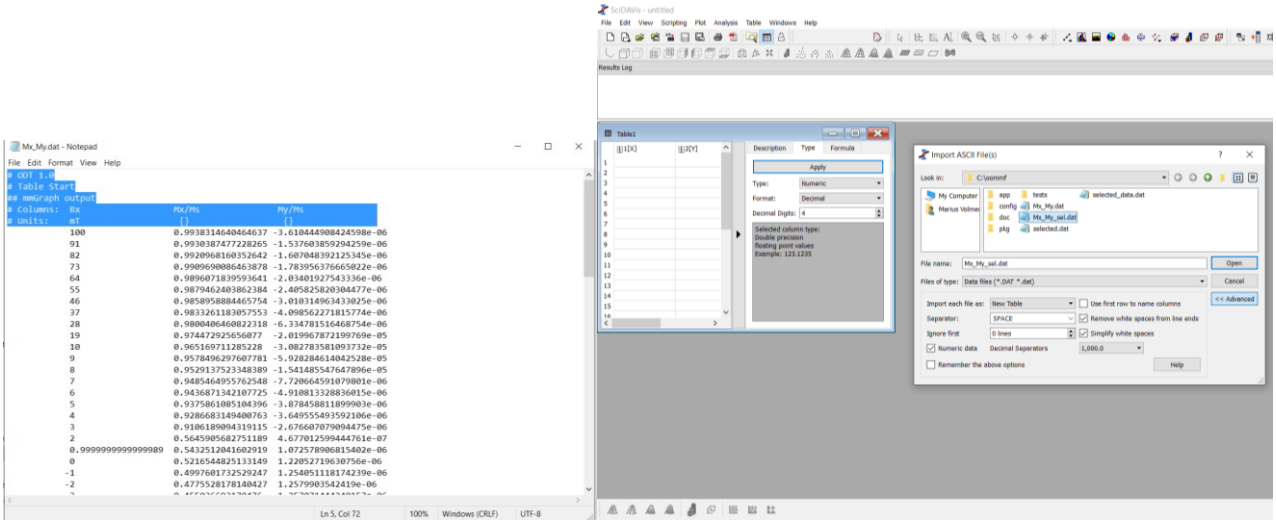

Fig. 7. Some simple steps to be followed to import the data file generated in OOMMF.

Before to plot data, give names to columns having the information from the original file. Fig. 8 shows the names and the roles assigned to each column. Also, it can be seen the measurement units. Note that for magnetizations the values are normalized to the saturation value, M_S, and the applied magnetic field is measured in mT. Finally, select both Mx/Ms and My/Ms columns and plot data selecting from the main menu Plot→Panel→Stacked Layers or Plot→Panel→Vertical 2 Layers, Fig. 8. By doing double click on x or y Axis Title you can label them. Doing the same, it can be changed the x and y axis scaling.

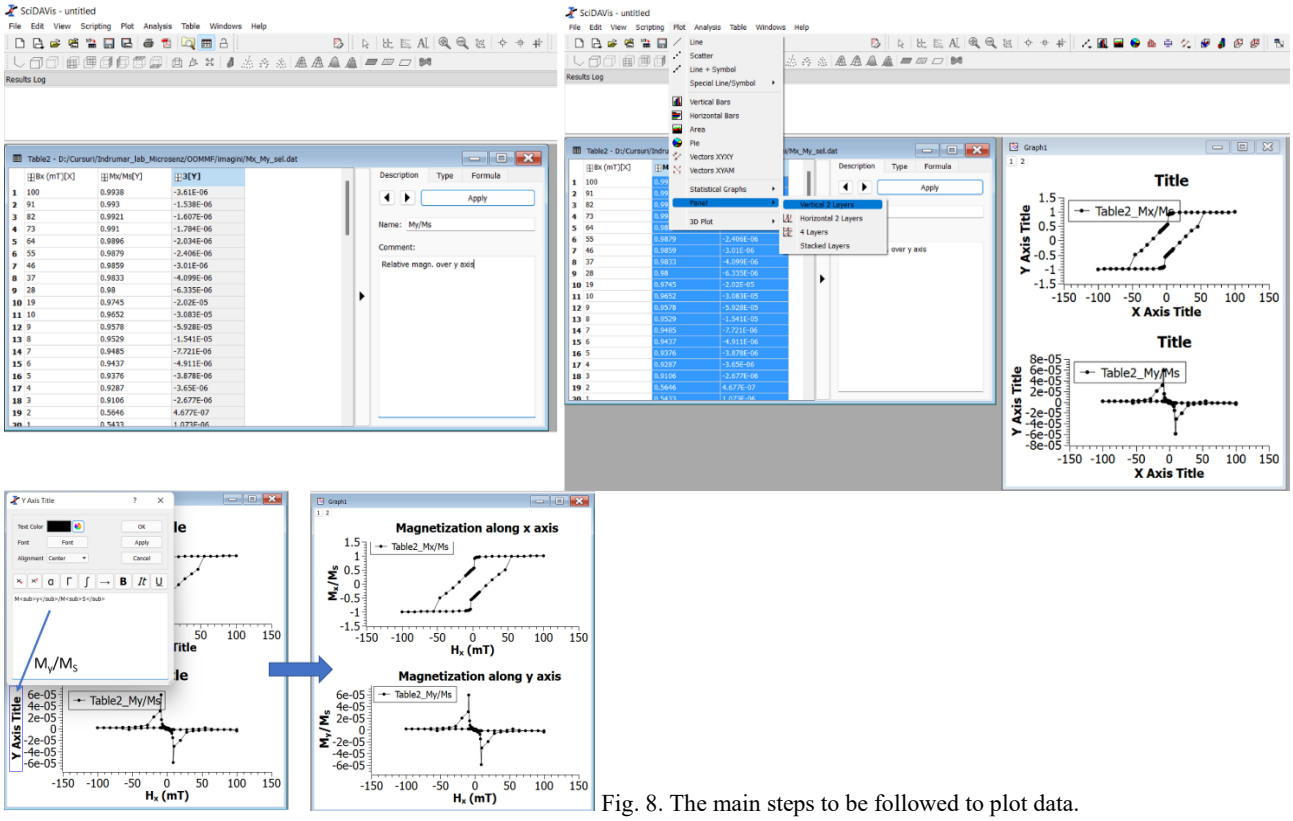

Fig. 8. The main steps to be followed to plot data.

Run simulations with simple geometrical structures that can be defined in OOMMF, like squares, rectangles, disks, or import masks with different geometrical shapes drawn, by example, in PowerPoint.

III. Study of a force senzor

1. Introduction

Force sensors are devices that are designed to translate applied mechanical forces, such as tensile and compressive forces, into output signals whose values can be used to reflect the magnitude of these forces. Modern force sensors deliver an electrical signal which can be further amplified, applied to a DAQ board, recorded, etc. In this practical work it is studied a piezoresistive strain sensor

2. Theoretical aspects

The general structure of a force sensor is presented in Fig. 1 which means that, usually, we talk about a complex sensor. Transducer 1 transforms the force, signal S_1, in a deformation – signal S_2. This is possible by applying the force to an elastic element like a cylinder, cantilever see Fig. 1, membrane, etc., such that $S_2=k_1S_1$.

Usually, this process obeys the Hooke's law:

$$\sigma = \frac{F}{A} = E\frac{dl}{l} \tag{1}$$

where σ represents the stress (tensor), F is the applied force, A is the cross section, E is the Young's modulus and *dl* is the deformation of the sensor of length, *l*.

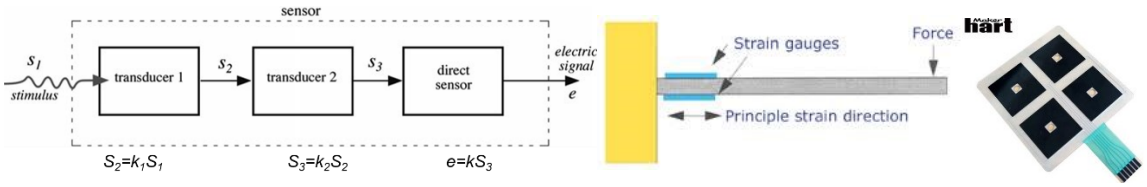

Fig. 1. The general structure of a complex sensor

The deformation of the elastic element is read by the transducer (sensor) 2, named *strain sensor* (or *strain gauge*) which returns a signal as a *voltage change* (for piezoelectric sensor) or as *resistance variation*, *dR*, (for piezoresistive sensor) expressed by:

$$\frac{dR}{R} = \frac{d\rho}{\rho} + \frac{dl}{l} - \frac{dA}{A}, \quad \frac{dR}{R} = \frac{d\rho}{\rho} + \varepsilon(1+2\mu), \quad \frac{dl}{l} = \varepsilon, \quad R = \rho\frac{l}{A} \tag{2}$$

where ε is called strain, which is a normalized deformation of the material, whereas μ is called Poisson coefficient that describes the transverse deformation; *dρ/ρ* represents the piezoresistive effect.

For elastic deformation, one can express:

$$\frac{dR}{R} = S_g \cdot \varepsilon \tag{3}$$

where S_g is gauge factor or sensitivity of the strain gauge element; S_g=2-6 for metallic resistors and S_g= 40-200 for semiconductors but the thermal stability is poor.

For resistive sensors, *dR*>0 for tensile forces because *dl*>0 whereas *dR*<0 for compressive forces because *dl*<0.

The general structure of the strain gauge, like the gauges used in this practical work, is presented in Fig. 2.

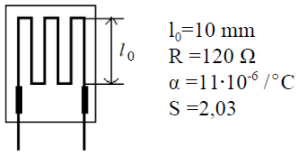

Fig. 2. A 10/120 LY – Hottinger strain sensor; note that for Cu α=3.86·10^{-3} /°C.

The old models were made of wire but the modern ones are etched onto a plastic backing material in a similar manner to how the tracks are etched on a printed circuit board. The difference is the backing material for a strain gauge is as thin as possible. The *gauge is glued* intimately to the item (transducer 1 in Fig. 1) and it is measuring the strain in. The conductive stripe is *very long and thin and is laid out with most of its length in one direction*, Fig. 2. Because of its dimensions it has an electrical resistance which is usually of 120 Ω or 350 Ω. When the gauge is stretched in the long direction the wire becomes longer which causes its resistance to increase. This small change in resistance is detected by a Wheatstone bridge, Fig. 3. In order to improve the thermal stability and to increase sensitivity of the output signal when a deformation is applied, different strategies are applied, Fig. 3. One used setup is the "half-bridge" when the Wheatstone bridge consists from two "active" arms made from identical strain sensors glued on the elastic element and other two strain sensors or simply resistors are used to complete the setup. However, if it's possible, it is desirable that all four arms of the bridge to be made from "active" strain sensors electrically connected and mechanically glued on the elastic element such that their resistance variation with deformation to be added. This is the most sensitive setup which, in the same time, offers the best thermal stability, Fig. 3. Rarely is used the "quarter-bridge" setup when only one arm contains an active sensor. Such setup offers a bad thermal stability and is often used for dynamical strain measurements where the useful signal can be separated from the slow temperature variation of the resistance of the strain sensor.

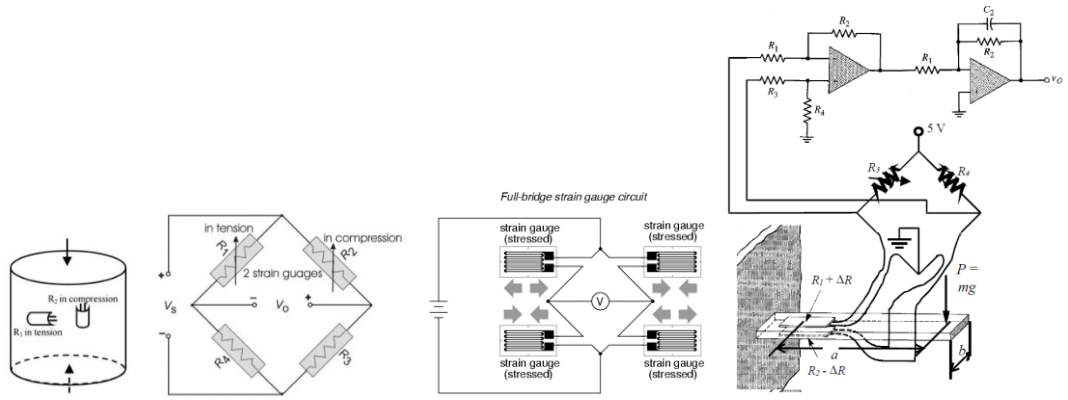

Fig. 3. "Half-bridge", "Full-bridge" strain gauge circuit and a typical example when a load is applied at the free end of the beam.

In function of the number, *n*, of "active" sensors used for detection, the output signal can be expressed as

$$U_{out} = U_S \frac{n}{4} S_g \qquad (4)$$

For a half-bridge, *n*=2, whereas for a full-bridge *n*=4; U_S is the supplied voltage applied to the bridge.

3. The experimental setup

The force sensor is presented in Fig. 4 and is composed from the strain sensors which are glued on a ring-shaped elastic metallic stripe. Fig. 4. shows the physical positions of sensors and the Wheatstone bridge configuration. A small permanent cylindrical magnet is attached at the lower part of this ring. Beneath the magnet is place a solenoid which can produce a magnetic field.

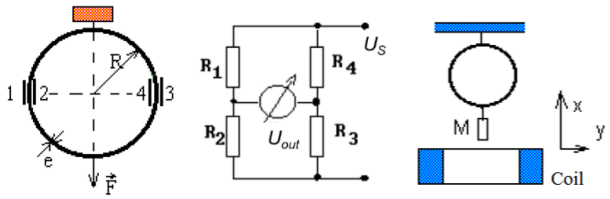

Fig. 4. The force sensor and the illustration of the real positions of the strain sensors $R_{1,2,3,4}$ in order to obtain a signal due to the applied force, *F*; R=210 mm, e=0.5 mm, a=30 mm – the stripe width.

This setup is used to detect small forces. The bridge can be supplied either by a DC or AC voltage or current. In our experiment the bridge is connected to a constant DC current source, K6221, and the output signal is read by a high sensitivity voltmeter, e.g., K2182A which can perform the offset correction due to the

bridge initial unbalance. The solenoid can produce a non-uniform magnetic field that can interact with the magnet. The interaction force can be measured after the sensor calibration.

The output voltage is:

$$\left.\begin{aligned} U_{out} &= 4 \cdot I \cdot R \frac{\Delta R}{R} = 4 \cdot I \cdot R \cdot S_g \cdot \varepsilon \quad (n=4) \\ \varepsilon &\sim F \end{aligned}\right\} U_{out} = k \cdot F \qquad (5)$$

The transfer coefficient, k, can be determined during the sensor calibration

On the other hand, the interaction force between the magnet and the solenoid is expressed by:

$$\left.\begin{aligned} \vec{F} &= -VM \frac{d\vec{B}}{dx}, \\ \vec{B}_i &= \mu_0 \vec{M} \end{aligned}\right. \qquad (6)$$

where V=3.18·10^{-7} m^3 is the volume of the magnet and M is his remnant magnetization; dB/dx is the field gradient. B_i is the internal magnetic flux density and μ_0=4π·10^{-7} N/A^2 is the vacuum magnetic permeability.

4. The experimental procedure

I. Sensor calibration

The current source is K6221 and the nanovoltmeter K2182A plays the role of the instrumentation amplifier and the offset correction circuit. Also, can be used a simpler setup which consists from a DMM with four wire resistance measurement capability and offset compensation. The drawback is that the current through the strain sensors cannot be adjusted.

a) A current I<20 mA will be set through the bridge using K6221;
b) A mass m_0<20 g will be placed on the lower part of the ring (where the force F is illustrated) in order to pretension the elastic element;
c) Using the ”Rel” switch from the nanovoltmeter front panel the initial reading is compensated so the displayed value is 0;
d) Calibrated weights, with mass m between 5 to 30 g, will be placed over the mass m_0; the displayed reading, U, will be recorded in a data table;
e) The calibration curve $U(F)$ will pe plotted and the transfer coefficient k will be calculated from the slope of the trend line; $F=m \cdot g$ (g=9.81 m·s^{-2});
f) An unknown mass will be placed over m_0 and the reading is recorded in the data table; the value of this mass will be calculated from the calibration curve
g) The current I will be changed to a higher value I’=2·I but not exceeding 40 mA;
h) The steps b → f will be repeated
i) It is recommended to plot on the same graph both calibration curves.

II. Measuring the remnant magnetization, M, of a permanent magnet

Will be used the setup from Fig. 4 when the mass m_0 is placed on the force sensor and the established current is I’ and calibration curve is built.

a) A solenoid will be used to generate the interaction force between the field gradient dB/dx and the magnetic moment $m=M \cdot V$ of the permanent magnet;
b) The calibration curves B(I_H) and B(x) for I_H=const. will be obtained using a digital teslameter; x is the distance from the upper surface of the solenoid (see fig. 4) and varies between 0 and 2 cm;
c) From the trend curve of the dependence (2nd order polynomial function) used to fit the data will be derived the expression dB/dx (field gradient). As an alternative, the calibration curves B(I_H) and B(x) for I_H=const. can be provided – see the examples on data handling;
d) The solenoid is placed beneath the force sensor, like in Fig. 4;
e) Will be checked the zero reading;
f) A current I_H=1 A will be established through the solenoid and the reading will recorded in the data table;
g) The same will be done for I_H=-1 A. Explain the behaviour of the data recorded;

h) From the sensor calibration curve will be calculated the forces F that act on the magnet for I_H=1 A and I_H=-1A;
i) The field gradient dB/dx will be calculated for x=1.1 cm (the distance between the upper surface of the solenoid and the middle of the magnet) and I_H=1 A;
j) Using eq. 2 will be calculated the modulus of the remnant magnetization M
k) Calculate the remnant internal magnetic flux density, B_i;
l) Discuss the observed behaviour of the magnet in applied field and of the displayed data;

In what follows are presented some examples on data handling for this complex practical work

a. Solenoid calibration

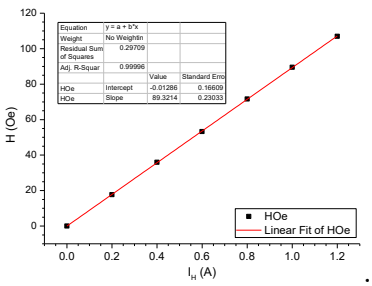

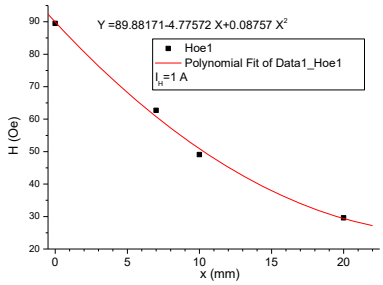

$$\frac{dB}{dx} = -4.77572 + 2 \cdot 0.08757 \cdot x \ \left[\text{Oe/mm}\right]$$

b. Remnant magnetization calculation for the attached magnet

For x=11 mm and I_H=1 A:

$$\frac{dB}{dx} = -2.84918 \ G/mm = -2.84918 \frac{10^{-4}\,T}{10^{-3}\,m} = -0.284918 \text{ T/m};$$

- in air 1 G=1 Oe
- but 1 T=10^4 G

For x=11 mm, I_H=1 A ➔ F_1=-0.03166 N
For x=11 mm, I_H=-1 A ➔ F_2= 0.03352 N

$$\vec{F} = -VM\frac{d\vec{B}}{dx} \Rightarrow |M| = \frac{F}{\left|\frac{dB}{dx}\right| \cdot V}$$ ➔ M_1=349432.99 A/m ➔ B_i=0.44 T; M_2=369961.90 A/m ➔ B_i=0.46 T

Data table - example

	mg	FN(X1)	UmV10(Y1)	UmV20(Y1)	k10mA	k20mA	UxmV	mxg	IemA	UmVmagn(	F	MAm	BiT	IemA1(X2)	HOe(Y2)	xmm(X3)	Hoe1(Y3)
1	0	0	0	0			0.041	0.00778	1	-0.017	-0.03166	349432.99	0.44	0	0	0	89.5
2	5	0.04905	0.014	0.028	0.28	0.537	0.032	0.00607	-1	0.018	0.03352	369961.9	0.46	0.2	17.7	7	62.7
3	10	0.0981	0.029	0.053										0.4	36	10	49.1
4	15	0.14715	0.042	0.081										0.6	53.26	20	29.6
5	20	0.1962	0.055	0.1										0.8	71.6		
6	30	0.2943	0.083	0.161										1	89.5		
7														1.2	107		

Additional tasks

1. Present some applications of force sensors based on piezoresistive effect;
2. Present some commercial models of strain sensors;
3. Present the using of a strain sensor with the Arduino board.

IV. Study of temperature microsensors

1. Introduction

Temperature sensors are devices that measure the temperature of the monitored system and convert the input signal into electronic data to record, monitor, or signal temperature changes. There are many different types of temperature sensors. Some temperature sensors require direct contact with the physical object that is being monitored (contact temperature sensors), while others indirectly measure the temperature of an object (non-contact temperature sensors) through the radiation emitted by this. Here we study contact temperature sensors based on (i) Seebeck effect (energetic sensors) and (ii) on variation with temperature of the voltage across a pn junction (parametric sensors). Note that in this practical work are studied fundamental aspects regarding the physical working principle, circuits for signal conditioning and DAQ, static and dynamic characteristics of these temperature sensors.

2. Theoretical aspects

2.1. Thermocouple

The thermocouple uses the Seebeck effect (more generally known as thermoelectric effect). In order to observe thermoelectricity, it is necessary to have a circuit composed of *two junctions* between two *different materials*, A and B, placed at *different temperatures*, T_{sense} and T_{ref}, like in Fig. 1. Can be used both metals and/or semiconductors. However, for applications devoted to measure temperature, A and B are metals. For applications devoted to build thermoelectric generators, A and B are semiconductors.

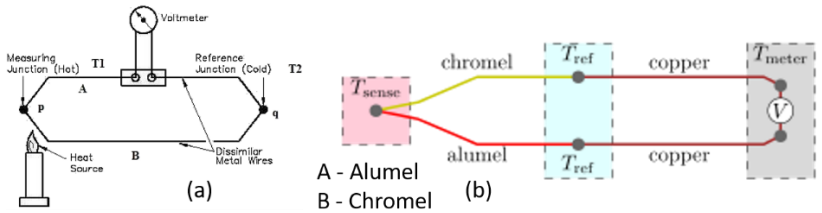

Fig. 1. (a) The general setup used to study the thermoelectric effect and (b) example of practical implementation – thermocouple.

The voltage generated by this setup is:

$$U_{AB} = S_{AB}\left(T_{sense} - T_{ref}\right) = S_{AB}\left(\theta_{sense} - \theta_{ref}\right) \quad (1)$$

where S_{AB} is named Seebeck coefficient and depends on the nature of materials A and B; θ is the temperature in centigrade degrees.

To characterize the metals from thermoelectric point of view, the metal "A" is Pt at 0 °C (reference temperature) and metal "B" to be characterized is at 100 °C. Using this pair of metals, a thermocouple can be built, Fig. 1, and some results are summarized below:

Constantan (Const)	-3.47...-3.04 mV
Nickel (Ni)	-1.94...-1.20 mV
Iron (Fe)	+1.87...+1.89 mV
Nickel Chromium (NiCr)	+2.20 mV

We observe that some metals are "electropositive" whereas other metals are "electronegative" referred to Pt. This data offers a guide to select metals to build thermocouples. The selection considers both sensitivity, temperature range and price (metals like Pt, Ru are very expensive). For example, a pair Iron-Constantan offers a voltage of about 5 mV for a temperature difference of 100 degrees between sense and reference junctions. This means that S_{AB}=0.05 mV/K=50 µV/K. For a pair like **Chromel** (90% nickel and 10% chromium) **Alumel** (95% nickel, 2% manganese, 2% aluminium and 1% silicon), known as K-type thermocouple, S_{AB}=41 µV/°C. K-type thermocouple is used for temperatures below 1000 °C. We see that chromel (NiCr) is positive relative to alumel (Ni) when the measurement junction temperature is higher than the reference temperature. From practical point of view, the metals used for connection to the measurement device are made from Cu but care must be taken to have an isothermal connection box for junction at T_{ref}.

Because U_{AB} depends on T_{sense}-T_{ref} , the voltmeter reads 0 when both junctions have the same temperature, for example room temperature. To overpass this issue different methods are used like (i) the reference junction is inserted in water with melting ice (0 °C) or (ii) is simulated by electronic means a "cold junction" at 0 °C. This method is mostly used in DAQ systems and digital multimeters. There are some special electronic circuits designed to amplify the voltage from thermocouple and can emulate a cold junction at 0 °C, named cold-junction compensation functionality. One can mention MAX31855 or MAX6675 circuits which are calibrated for K-type thermocouple, have the cold-junction compensation functionality and deliver directly at output a digital signal. However, these circuits will deliver wrong results for other thermocouples. Also, note that some thermocouples have a nonlinear voltage-temperature characteristic and a calibration curve must be obtained.

In this practical work will be characterized a K-type thermocouple.

2.2. The pn junction temperature sensor

The voltage across a pn junction, Fig. 2, depends with temperature.

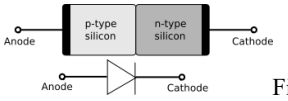

Fig. 2. Illustration of a pn junction.

The I-U characteristic is expressed by:

$$I = I_S\left(e^{\frac{qU}{K_BT}} - 1\right) \tag{2}$$

where I_S is the saturation current, U is the applied voltage, q=1.6x10^{-19} C is the electron charge, K_B is the Boltzmann constant (K_B=1.38x10^{-23} J/K) and T is the absolute temperature.

When U<0 (reverse bias), I≈-I_S if U is large enough. When U>0, forward bias, eq. 2 becomes, according to A.S. Grove and Mell-Ross theory:

$$I = I_S \cdot e^{\frac{qU}{K_BT}} \approx const. \cdot T^n e^{\frac{q}{K_BT}\left(U - \frac{E_g}{q}\right)} \tag{3}$$

where E_g is energy bandgap; E_g = 0.5 -1 eV and n is a material parameter; n=1.5 for Si

If we consider forward biasing at a constant current, I, we find:

$$U = n\frac{K_BT}{q}\ln\frac{T_0}{T} + U_0\frac{T}{T_0} + \frac{E_g}{q}\left(1 - \frac{T}{T_0}\right) \tag{4}$$

where U_0 is the voltage at a reference temperature, T_0, chosen in a convenient way (example, T_0=273.15 K).

Both from eq. 4 and from experiment is found a quite linear dependence of the voltage in function of temperature with a negative slope between -0.002 to -0.004 V/K, in function of the junction structure and driving current. This property can be used for temperature sensing for 1 K < T < 400 K. Only special pn junctions with SiC can sustain temperatures larger that 400 K. Usually, such sensors are used for low temperatures up to 300 K.

A simple electronic thermometer consisting from two current sources and a pn diode is presentd in Fig. 3. As a pn junction sensing element is used the B-E junction from a transistor in metalic case.

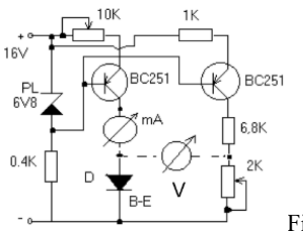

Fig. 3. Schematic illustration of an electronic thermometer with pn junction

2.3. The bandgap temperature sensor

The bandgap temperature sensor is an integrated circuit (IC) sensor which contains as sensing elements two pn junctions supplied at different biasing currents. Usually, the output voltage is a function of the absolute temperature allowing building of IC temperature sensors like LM335 (operates in K), LM 35 (which operates in °C), LM75, etc.

In this practical work is used the temperature sensor LM335.

Some main features of this sensor are:

- precision, easily-calibrated, integrated circuit temperature sensor
- LM335 operates from −40°C to 100°C
- **Directly calibrated in Kelvin**
- voltage directly proportional to absolute temperature at +10 mV/°K
- low impedance and linear output

The pins configuration and the circuit connection are presented in Fig. 4.

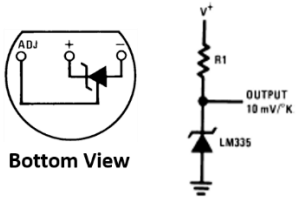

Fig. 4. The temperature sensor LM335

Usually, the polarization resistor, from Fig. 4, is between 1-3 kΩ for a supply voltage of 5 V. The output characteristic of this sensor is:

$$U_{outT} = U_{outT_0} \times \frac{T}{T_0} \tag{5}$$

where U_{outT0} is the output voltage for the reference temperature T_0.

3. The experimental setup

Three temperature sensors as K-type thermocouple, pn junction (B-E junction from a bipolar n-p-n transistor) and an integrated sensor LM335 are connected to a LabJack U12 DAQ system, like in Fig. 5. For more details concerning this system, see the practical works devoted to study the GMR and Hall effect magnetic microsensors. Also, useful info can be found at https://labjack.com/.

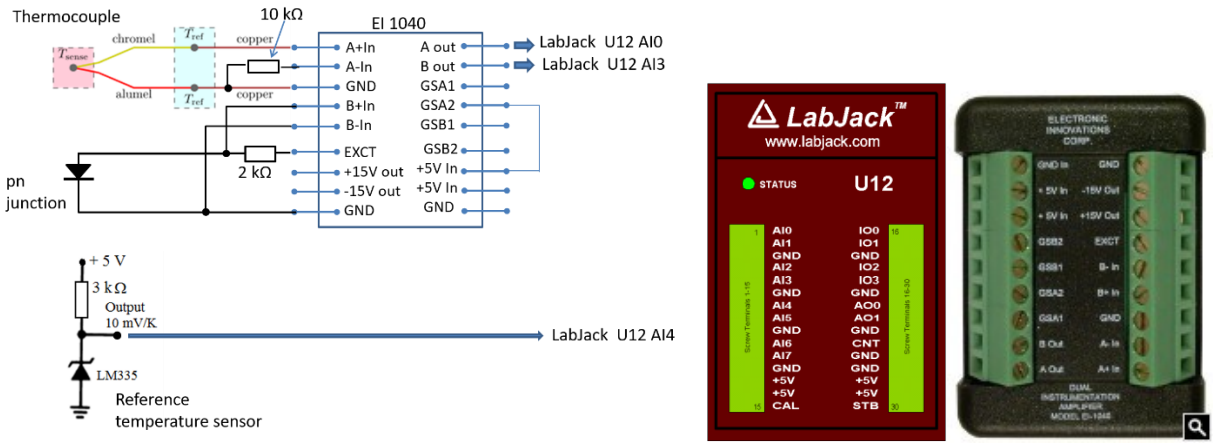

Fig. 5. The circuit schematics and sensors connection. Are presented the DAQ board and the instrumentation amplifier EI 1040.

The signal from thermocouple is amplified by 100 times (5 V applied on GSA2 ➔ G_A=100) whereas the signal from the pn junction is amplified by1 time (GSB1 and GSB2 are in 0 logical state) or by 10 times (5 V applied on GSB1 ➔ G_B=10). The LM335 sensor is connected directly to DAQ board and has the role of a reference sensor used for calibration of thermocouple and pn junction temperature sensors. The pn sensor is supplied with a stable voltage of 4.096 V, provided by the excitation output from EI1040 instrumentation amplifier.

The conditioned signals, from Output A and B, will be applied to the Analog Inputs (AI) of the DAQ board LabJack U12, Fig. 5. AI 1 and AI 5 will be connected to ground; AI 2 will be connected to AO0 (analog output) of LJ U12; AO0 can provide a programmable DC voltage used to compensate the voltage from the pn junction at the reference temperature. By this, the LJ U12 analog inputs AI0-AI1, AI2-AI3 and AI4-AI5 can be configured in a differential setup which assures a higher input impedance and adjustable gain.

To perform the measurements will be used the following applications:

- LJlogger – logger used to aquire data during sensors calibration;

- LJstream – application used to make high-rate data acquisition for determination of the time constants.

4. The experimental procedure

a) The temperature sensors, connected like in Fig. 5, will be inserted in a glass with water at room temperature – this will be considered as the reference temperature during the experiments;
b) The output of AO0 will be set until the voltage applied to AI2 will be equal with the voltage applied to AI3. Now, the reading of AI2-AI3 differential channel will be 0;
c) A reference thermometer will be used to check the reading of the LM335 sensor used also as a reference sensor during calibration procedure;
d) Now, the temperature sensors will be placed in a second glass with water, at the same temperature, which can be heated. The heater will be turned on;
e) Using the Ljlogger application (see the works devoted to study GMR and Hall effect magnetic microsensors), the data from these sensors will be recorded at a rate of 1 reading at every 15 s. The data will be stored in a file which can be opened with Excel, Origin, Graph or SciDAVis dedicated programs;
f) The heater will be turned off at 60 °C and the data recording will be stopped;
g) The sensors will be removed from the heated water an after 5 min will be placed in the water at room temperature;
h) The LJlogger application will be closed and the LJstream application will be opened. Use ”Configure channels”, ”Change working directory” and ”Data file prefix” settings. A scan rate of 100 readings/s will be used;
i) Press ”Enable stream”. The program will start to acquire data;
j) The sensors will be moved rapidly from water at room temperature to hot water. This is equivalent with a square temperature signal applied to sensors. The system will record the time dependence of the sensors output;
k) Stop the measurements after 60 s;
l) Using the data file generated by LJlogger, plot the dependences U_{01}=f(U_{45}) and U_{23}=f(U_{45}). U_{01} is the voltage from thermocouple, U_{23} is the voltage from the pn junction and U_{45} is the voltage from the reference sensor, LM 335. In the “Multiplier” Tab from LJlogger measurement window, multiply the read data from LM335 (line SD2, AI4-AI5 channel) with 100 to have an output directly in K displayed in “Scaled Data”;
m) For each plot determine the slopes of the trend lines S_{01} and S_{23} which represent the sensitivities of the thermocouple and pn junction temperature sensor, respectively;
n) Using the data recorded by LJstream, plot the time dependences U_{01}=f(t), U_{23}=f(t) and U_{45}=f(t). Determine, using the procedure from Fig. 6, the time constant, τ, for each sensor and note these values on the corresponding plot;
o) Give a brief discussion on the obtained results: which is the most suitable sensor for particular applications (temperature range, easy to use, small response time, etc.).

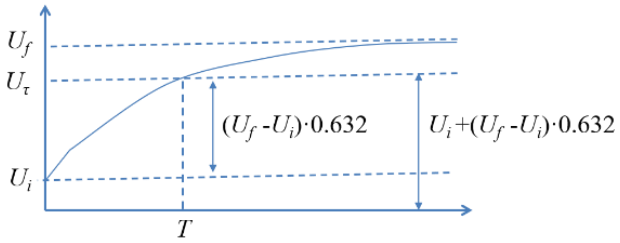

Fig. 6. Typical time dependence of the output signal of a temperature sensor subject to a square shape applied temperature

For exemplification, Fig. 7 shows typical plots of the dependences U_{tc}=f(T) and U_{pn}=f(T) whereas Fig. 8 shows the output signals U_{01}, U_{23} and U_{45} in function of time, measured in conditions described above. These plots can be used to validate the obtained results.

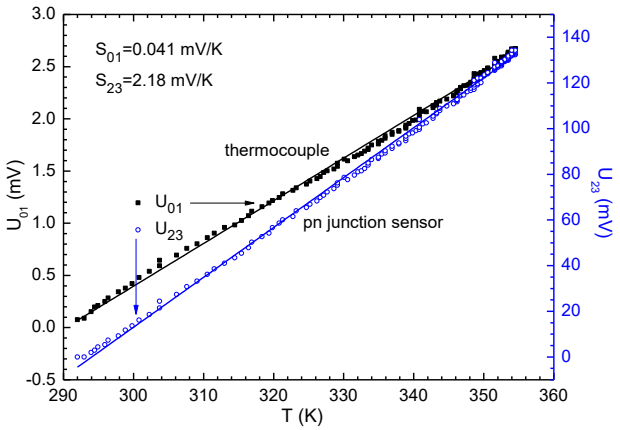

Fig. 7. Static characteristics of sensors: typical plots of the dependences U_{01}=f(T) and U_{23}=f(T)

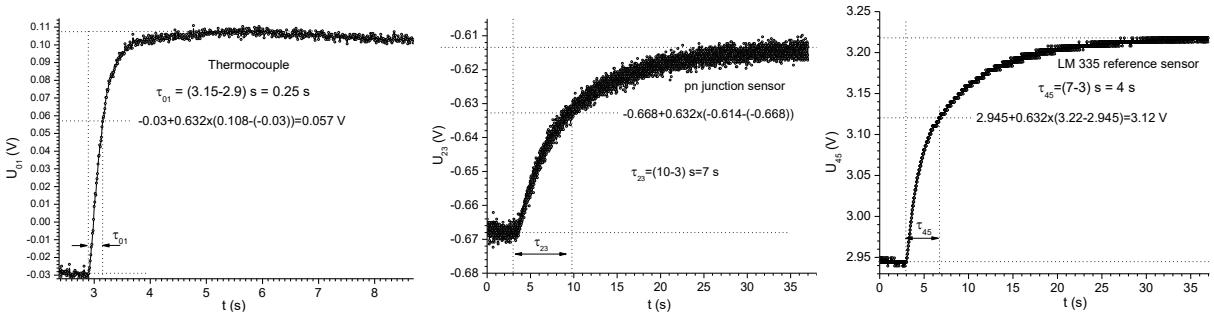

Fig. 8. Dynamic characteristics of sensor: typical plots of the output signals in function of time measured with LJstream

Proposed project

Try to build an Arduino based temperature measurement system which is using a K-type thermocouple and the amplifier MAX31855/MAX6675. A proposed detailed wiring schematics is presented in Fig. 9 (https://www.instructables.com/Thermocouple-Amplifier-and-K-Type-Thermocouple-Int/).

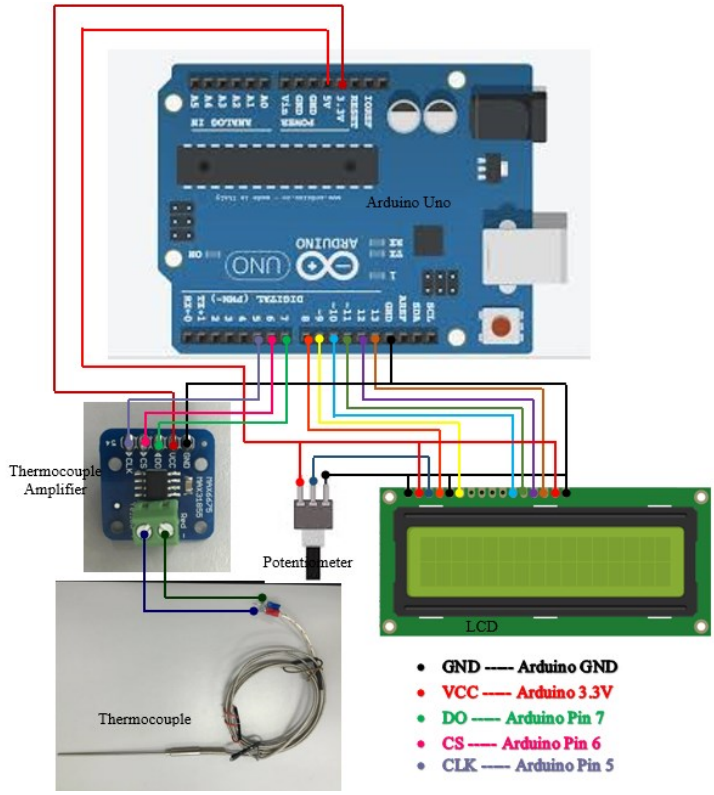

Fig. 9. Thermocouple amplifier and K-Type thermocouple interface with Arduino. The circuit can be simulated on https://wokwi.com/

V. Study of Hall effect microsensors

1. Introduction

Hall effect microsensors are used to detect magnetic field and have a broad range of applications as magnetometers, controlling brushless DC motors, etc. Besides practical applications, the Hall effect is a very powerful tool for material characterization, allowing the estimation of carrier density in semiconductors and of the conduction type (n or p).

2. Theoretical aspects

The Hall effect was discovered in 1879 in Johns Hopkins University by E. H. Hall in a nonmagnetic metallic plate, Fig. 1. Because of the Lorentz force, the moving electrons trajectory is altered in applied magnetic field such that one side becomes negatively charged whereas the opposite side becomes positively charged. When the internal electric field, E_H, generates a force $\vec{F}_H = q\vec{E}_H$, that cancels the Lorentz force, $\vec{F}_L = q \cdot \vec{v} \times \vec{B}$, a Hall voltage, $U_H=V_{H+}-V_{H-}$, appears. The polarity of the generated voltage depends on the current and magnetic field directions and can be found from the orientation of the Lorentz force. See, for example, the polarity of the Hall voltage in Fig. 1.

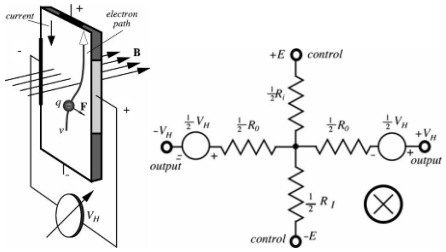

Fig. 1. Schematic of the Hall effect setup and the equivalent circuit of a Hall sensor

Based on the above considerations, the Hall effect voltage can be expressed by:

$$U_H = R_H \frac{I}{t} B \qquad (1)$$

where R_H is a parameter material named Hall constant, I is the driving current through the structure, t is the thickness of sample whereas B is the applied magnetic flux density.

For thick metallic layers, like that used by E. Hall, the signal was too weak to inspire practical applications such that when the Hall effect was discovered did not present an interest for practical applications. However, in thin semiconductive layers, the amplitude of the Hall voltage is much larger than in metallic layers with the same thickness. This is because $R_{H,\ semiconductors} >> R_{H,\ metals}$.

Equation 1 shows a linear dependence of the Hall voltage in function of the applied magnetic field. The Hall voltage has a maximum value when B is perpendicular on the plate surface, and hence on the driving current, and is 0 when B is parallel with the current (there are no longitudinal effects). Also, the Hall voltage takes into account the orientation of B. Such that the Hall effect can be used both for (i) research to study materials through R_H which describes the type of conduction in semiconductors and the magnetic behaviour of the material and (ii) for practical applications like for magnetic field sensing, etc.

The Hall effect sensors are fabricated using IC technology. Various types of sensors can be found on the market, like basic sensors, as presented in Fig. 1, and the integrated sensors that contain electronic circuits for signal procesing, etc. For example, the Hall I.C. sensor UGN-3605K manufactured by Sprague, has a sensitivity of 60 μV/Gauss.

3. The experimental setup

In this practical work is characterized a Hall effect microsensor. The measurement system is composed from:

- Hall sensor;

- DAQ system based on a LabJack U12 board and EI 1040 dual channel signal conditioning circuit;
- Power supply source
- Solenoid

The basic schematics of the measurement system is presented in Fig. 2. Please identify the parts and try to explain their role.

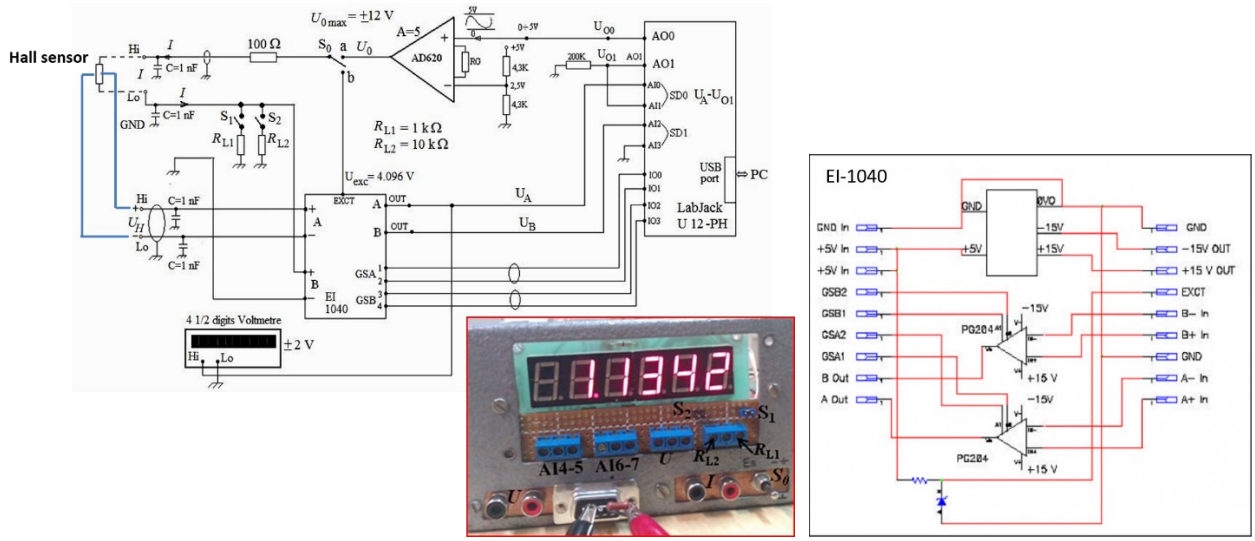

Fig. 2. The basic schematics of the DAQ system and details of the internal structure of EI 1040 2 channels PGA

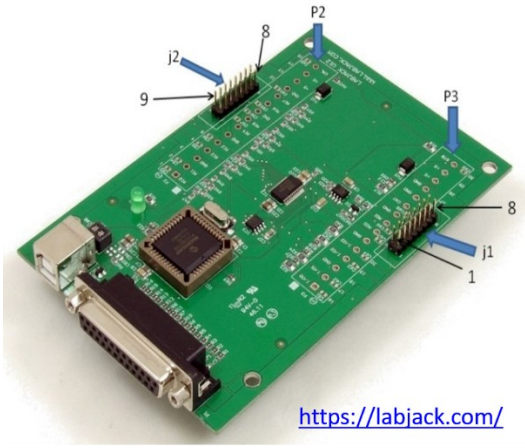

J1	J2
1 IO0	1 AI0
2 IO1	2 AI1
3 GND	3 GND
4 IO2	4 AI2
5 IO3	5 AI3
6 GND	6 GND
7 AO0	7 AI4
8 AO1	8 AI5

Fig. 3. LabJack DAQ U12 DAQ board and pins description

The circuit from Fig. 2 has a controllable bipolar source (composed from AO0 and AD 620) where can be connected the sensor or other device under test (DUT) seen as a load, R_L. The current through sensor is the voltage read on R_{L1}=1 kΩ or R_{L2} = 10 kΩ, which can be selected by $S_{1,2}$, and applied to channel B of EI 1040. This voltage is applied to analog inputs AI2-AI3 of LJ U12. The Hall voltage is read on channel A, amplified and applied to AI0-AI1. The gain of A and B channels from EI 1040 can be digitally controlled through LJU12 digital I/O pins IO0-IO3. By using a load resistor of 1 Ω, connected between other analog inputs, AI4-AI5, see Figs 2 and 3, can be recorded the current which is flowing inside the solenoid. Such that with this setup can be: (i) set a driving current through the sensor, (ii) read the Hall signal and (iii) read the current and, hence, the magnetic field generated by the solenoid.

The LJ U12 analog inputs can be configured in differential setup channels as AI0-AI1, AI2-AI3 and AI4-AI5 which assures a higher input impedance and adjustable gain.

To perform the measurements will be used the LJlogger application, Fig. 4.

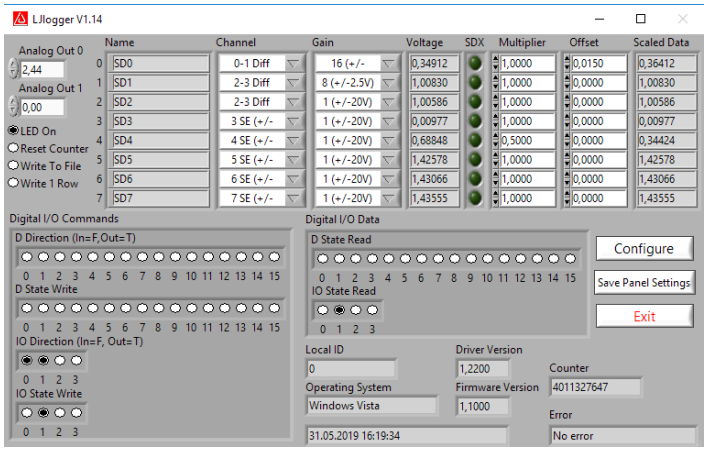

Fig. 4. LJlogger application; the gain for channels A and B from the PGA amplifier EI1040 can be set through „IO State Write" digital commands (see also Fig. 2). In this example, the gain of channel A is set to 100.

4. The experimental procedure

4.1. Sensor calibration

A programmable power source will be used to drive the current trough the solenoid from +1A to -1A with a frequency lower than 0.05 Hz. The Hall sensor is placed above a solenoid which generate a magnetic field H=I(A)x120 [Oe] or B=I(A)x0.012 [T]. The Hall signal and the current through the solenoid will be acquired by the DAQ system as described in section 3.

a) A current I=1 mA will be set through the Hall sensor using the setup from Fig. 2 where S_0 is in position "a" and S_1 is closed. This means that a load resistor R=1 kΩ is used to read the current I;
b) The gain for channel A is set to 100 whereas the gain for channel B is set to 1. This can be achieved from the front panel of LJlogger application, Fig. 4;
c) A magnetic field between + and -150 Oe (0.015 T in air) will be swept and the corresponding Hall effect signals will be acquired;
d) The same will be done for I_{sens}=2mA, 3 mA. Do not overpass 4 mA through sensor;
e) The calibration curves $U_{Hall}(H)$ or $U_{Hall}(B)$ will be plotted on the same graph and the corresponding sensitivities, S_H, will be calculated for each driving current using linear fitting method;

4.2. Current sensor with galvanic isolation

The Hall sensor is surrounded by a U-shaped metallic loop which can be connected to the programable power supply source using the same setup described above, by disconnecting from circuit the solenoid and connecting the metallic loop.

a) The current through Hall sensor is set to I=2 mA
b) The current I_l through the metallic loop will be swept between + and - 0.8 A and the U_{Hall}=f(I_l) signal will be recorded.
c) The calibration curve $U_{Hall}(I_l)$ will be plotted and the corresponding sensitivity, S_I, will be calculated using linear fitting method.

Typical plots of the Hall sensor calibration for two currents of 1 and 2 mA are shown below.

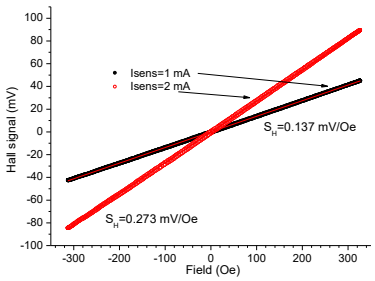

Additional tasks:

a. Give a brief discussion on the possible applications of the Hall effect.
b. How can be improved the S/N ratio of the measurements made for calibration of the current sensor?

VI. Magnetic field microsensors based on GMR effect

1. Introduction and theoretical aspects

The Giant Magnetoresistance Effect (GMR) effect in magnetic multilayers from thin-films was discovered separately in 1988 by Albert Fert, Baibich and coworkers at the Université Paris-Sud and by Peter Grünberg (Germany) on a Fe/Cr multilayer structure. Fert and Grünberg were awarded with Nobel prize in Physics.

In fact, the GMR effect can appear in many multilayered magnetic structures of the type FM/NM/FM; here FM denotes magnetic layers like $Ni_{80}Fe_{20}$, Co, CoFeB with thicknesses between 1 and 10 nm whereas NM denotes a nanometer thick conductive nonmagnetic spacing layer such as Cu or Ag which has the role to separate the FM layers that can interact between them by magnetostatic coupling or through exchange interaction due to conduction electrons. The physical mechanism of the GMR effect is the spin-dependent scattering at the FM/NM interfaces and in ferromagnetic layers for "*spin-up*" (*spin parallel to layer magnetization*) and "*spin-down*" (*spin antiparallel to layer magnetization*) electrons. Consequently, due to GMR effect, the structure resistance changes according to the angle between the directions of the magnetization of adjacent FM layers. When the layers are magnetized in parallel direction, the resistance is at a minimum value, R_p. When the magnetizations of the adjacent magnetic layers are antiparallel to each other, the resistance is at a maximum value, named R_{ap}, Fig. 1. This behaviour is important for designing practical applications. Because such structures are acting like filters for electrons in function of their spin orientation, they are known also as "spin-valve" structures.

The magnitude of the GMR effect is expressed by (1), and is typically between 5-15%.

$$GMR = \frac{R_{ap} - R_p}{R_{ap}} 100 \ [\%], \qquad (1)$$

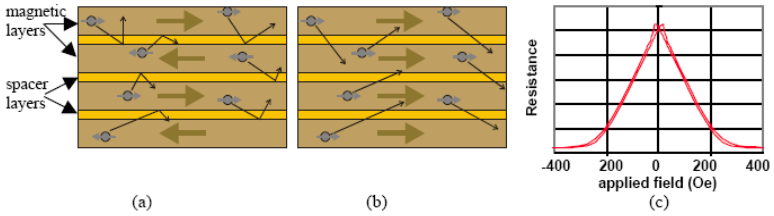

Fig. 1. Illustration of the GMR effect in magnetic multilayers: a) denotes the antiparallel (ap) state with a larger value of the structure resistance whereas b) shows the parallel (p) state configuration in magnetic layers with a smaller value of the structure resistance. The field dependency of the GMR effect is presented in c).

To have a workable structure, the magnetization of one ferromagnetic layer is pinned by an anti-ferromagnetic (AF) layer of FeMn or IrMn, and is named pinned layer (FM_{PL}), while the second FM layer has the magnetization free to rotate under the action of an external magnetic field and is named free layer (FM_{FL}). The magnetization of the FM_{PL} layer is pinned through an exchange interaction at the interface between the AF and the FM_{PL} layers. This interaction *manifests like a field*, named *exchange biasing field* (or *pinning field*), H_{pin}, applied only to FM_{PL}. Usually, H_{pin} ranges from 2 to 100 Oe. Such structure is of the type Substrate/Ta/FM_{FL}/NM/FM_{PL}/AF/Caping layer. The substrate consists of a single crystalline Si wafer on which a SiO_2 isolating layer is grown. The Ta layer assures the adhesion of the structure on substrate. Fig. 2 shows an "exchange biased spin-valve" structure and the simplified design used in simulations that help us to understand the field behaviour of the GMR effect.

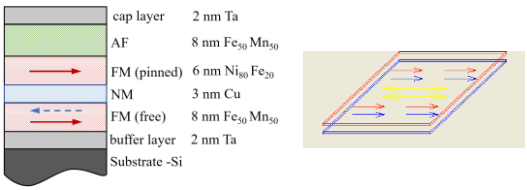

Fig. 2. An exchange biased spin-valve struture

The electrical resistance dependence on the angle θ, between the magnetizations of adjacent magnetic layers is expressed by:

$$R = R_p + \frac{\Delta R_{GMR}}{2}(1-\cos\theta) \qquad (2)$$

where R_p is the structure resistance at the saturated state i.e., when all magnetic moments have the same orientation (parallel); $\Delta R_{GMR}=R_{ap}-R_p$ is the amplitude of the GMR effect which depends on the properties of the magnetic layers. θ is the angle between the magnetization directions from two adjacent layers which, in turn, *depends on the magnetic field, H, applied in the film plane*, and on the system's properties like magnetic anisotropy, the coupling between the magnetic layers and the pinning field. By using the freeware program, Simulmag, one can study in single domain approximation (see the applications devoted to micromagnetic simulations), different types of magnetic multilayered thin films and simulate their GMR response in function of the applied magnetic field and his orientation. The simulated GMR structure is presented in Fig. 3 and consists from an exchange biased trilayer. The magnetization of one magnetic layer (marked with blue arrows) is pinned through exchange interaction with the AF layer, H_{pin}=200 Oe, whereas the magnetization from the sensing layer (red arrows) is free to rotate; note that the AF layer is not drawn by the simulator. Between the magnetic layers is defined a positive exchange coupling described by H_{coupl}=70 Oe which lowers the negative magnetostatic coupling between them – see the practical work devoted to micromagnetic simulations on thin magnetic layers. Fig. 3(a) shows the field dependences for magnetization and the GMR effect when the field is applied in the film plane, along the easy axis of magnetization. Note (i) the correlation between M and GMR and (ii) the two stable states when H=0 which can be attained by scanning the field from positive and negative orientations; see the arrows from Fig. 3(a). Such that, the structure can "memorize" two stable states with high resistance (R_{ap}) or low resistance (R_p) at zero field. This behaviour is applied for data storage, like MRAMs. On the other hand, the hysteretic effects are vanishing when H is applied in the film plane, perpendicular on the easy axis, Fig. 3(b). At zero field, *M* lies spontaneously along the easy axis in order to lower the magnetic energy. The corresponding behaviour is seen for GMR effect. This setup is mainly used for sensing applications. Note that (i) the sensitivity is very small around zero field, (ii) the field dependence of the GMR effect is nonlinear and (iii) for large fields, the GMR effect saturates.

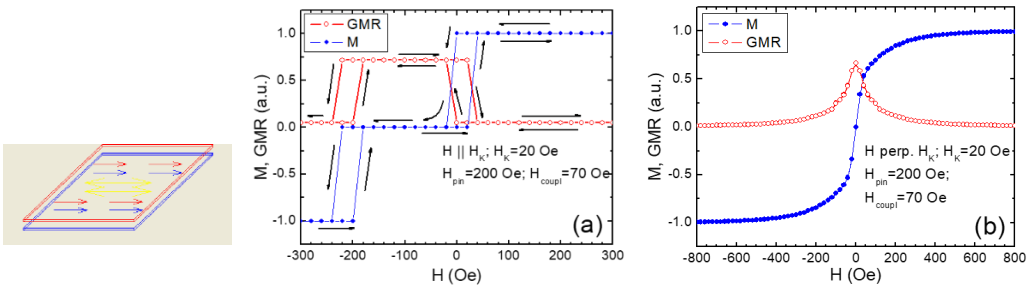

Fig. 3. Micromagnetic simulations with *SimulMag* for magnetization (blue) and GMR (red) curves when H is applied (a) along the easy axis and (b) perpendicular on the easy axis; with yellow arrows is shown, on the simulated structure, the anisotropy axis.

There are several methods to linearize the GMR field dependence around zero field. One method is based on spin-valve structures with crossed anisotropies, Fig. 4(a-c). Another method uses a small biasing magnetic field that brings the structure, see Figs. 2-3, in a linear region of the GMR effect. Fig. 4(d) shows the field behaviour of the GMR effect for a spin valve structure with crossed anisotropies.

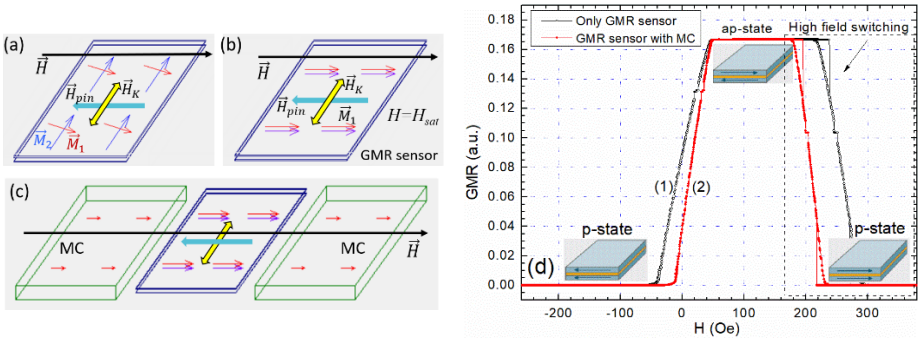

Fig. 4. A simulated spin-valve structure with crossed anisotropies shown (a) for a field $H<H_{sat}$, (b) at saturation and (c) with a built-in magnetic field concentrator. The results of micromagnetic simulations are shown in (d) only GMR sensor (1) and for GMR sensor

with magnetic flux concentrator (MC) – curve (2); p-states means that magnetizations have parallel orientations (left or right) and ap-states means that magnetizations have antiparallel orientations.

The simulated field dependency of the GMR effect, form Fig. 3(d), shows (i) a linear dependence around zero field and emphasizes the importance of the magnetic flux concentrator (MC) that increases the strength of the magnetic field inside the gap. Such sensors are used for small applied fields, between -100 Oe to 100 Oe. The MC consists from a soft magnetic material with a large magnetic permeability and low coercive field in order to minimize the hysteretic effects. For some practical implementations, the field inside the gap, where is placed the sensor, is about 10 times larger than the applied external field. In the same time this is acquired with the cost of some nonlinearities and hysteretic effects.

2. The experimental setup

2.1. Description of the used sensors

Two GMR based magnetic field sensors will be studied. They are working like was described through micromagnetic simulations in Section 1. The sensors are from Sensitec Germany: the sensor GF705 has a field characteristic like described in Fig. 3(b) whereas the sensor GF708 has a characteristic like in Fig. 4(d). These sensors are presented in flip-chip package, with a dimension of 1.4x0.9 mm^2.

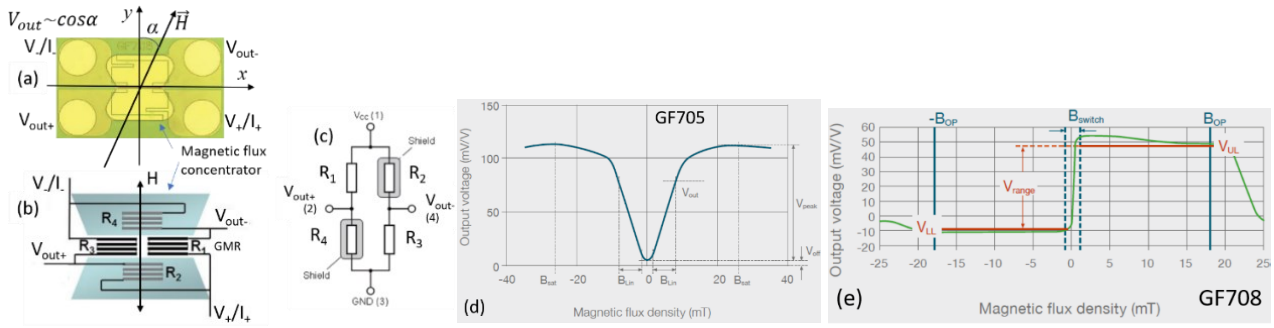

Fig. 5. (a) View of the sensor, GF705 or GF708, from the bump-side, (b) and (c) simplified schematic of the sensor with active GMR structures, $R_{1,3}$ and screened structures $R_{2,4}$; the maximum field sensitivity is reached when $\vec{H}$ is directed over y axis. The field characteristics are shown in (d) and (e) for GF705 and GF708 respectively (https://www.sensitec.com/service-support/download)

Both models (GF705, GF708) contain a Wheatstone bridge with on-chip flux concentrators to improve the field sensitivity and the thermal stability of the output voltage, Fig. 5(a-c). There are four identical GMR sensors on chip connected like in Fig. 5(b,c). Two of them are placed beneath the MC and screened to external field and the other two are placed inside the gap of the MC, see Fig. 4(c) and Fig. 5(b). At zero field, the GMR elements have almost the same value of their resistance and the bridge is balanced. The output voltage stays around zero with a small offset. When an external field is applied, R_1 and R_3 change their values according to Fig. 3(b) for GF705, and Fig. 4(d) for GF708, whereas R_2 and R_4, which are screened, will be unchanged. As a consequence, the Wheatstone bridge becomes unbalanced and an output voltage appears with a field dependence like in Fig. 5(d), for GF705, and like in Fig. 5(e) for GF708. For higher fields, the signal saturates. For GF705 is defined the linear region, Fig. 5(d), which is between 1.8 to 8 mT (18 to 80 Oe). For GF708 the linear operating range is determined by the magnetic switching range, Fig. 4(d) which is between -1mT to 1 mT (-10 to 10 Oe), Fig. 5(e). Table 1 summarizes the main characteristics of the sensor GF705.

Table 1. (from https://www.sensitec.com/fileadmin/sensitec/Service_and_Support/Downloads/Catalogue/Sensitec_Katalog2015_Web_LZen.pdf)

Symbol	Parameter	Conditions	Min.	Typ.	Max.	Unit
V_{CC}	Supply voltage		-	5	9	V
B_{LIN}	Linear magnetic flux density range (abs)		1.8	-	8	mT
B_{sat}	Saturation magnetic flux density [1]		-	±25	-	mT
S	Sensitivity (in linear range)	B = (1.8…8) mT	8	10	12	mV/V / m/T
R_B	Bridge resistance		4	5	7	kΩ
ε_{LIN}	Linearity error	B = (1.8…8) mT	-	1.5	3	% of V_{out}
ε_{Hys}	Hysteresis error		-	1	2.5	% of V_{out}

Table 2 summarizes the main characteristics of the sensor GF708 and Fig. 6 show a zoom of the field characteristic around zero where a small hysteretic effect is seen.

Table 2. (from https://www.sensitec.com/fileadmin/sensitec/Service_and_Support/Downloads/Catalogue/Sensitec_Katalog2015_Web_LZen.pdf)

Symbol	Parameter	Min.	Typ.	Max.	Unit
General					
V_{CC}	Supply voltage	-	5	9	V
R_B	Bridge resistance	13	16	19	kΩ
Switching applications					
B_{op}	Magnetic operation range	-18	-	18	mT
B_{switch}	Magnetic switching range	-1.0	-	1.0	mT
V_{range}	Electrical output range	30	56	70	mV/V
Magnetic field applications					
S	Sensitivity	80	130	160	mV/V/mT
V_{lin}	Linear range of output voltage	30	40	50	mV/V

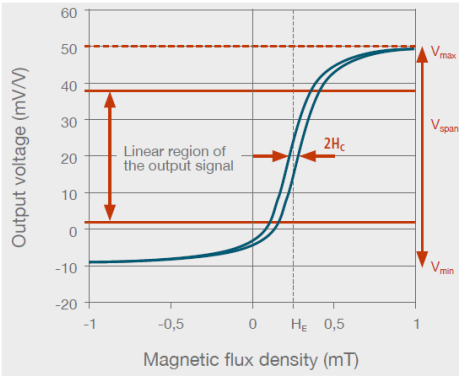

Fig. 6

These data allow us to estimate the output signal in function of the applied field and supply voltage. A higher supply voltage, a higher signal can be delivered but care must be taken for self-heating effects and the maximum current that can be driven through the sensors. Usually, the sensors can be supplied with a constant voltage but also the method of a constant supply current can be used.

2.2. The setup

From electrical point of view, a typical setup for a Wheatstone bridge or Hall effect sensor is used. The schematics of the experimental setup is presented in Fig. 6. It is based on a LabJack U12 DAQ board and EI 1040 dual channel signal conditioning circuit, https://labjack.com/. This DAQ board has 8 analog inputs (AI0-AI7) which can be configured as single ended or differential inputs (e.g., AI0 - AI1) and 4 digital input/output ports. The dual channel signal conditioning circuit has two differential inputs with digitally controlled gain (1 to 1000) and can deliver a very stable voltage, of 4.096 V, that can be used to supply sensors. More details can be found, also, in the description of the experimental setup used to study Hall effect microsensors or temperature sensors presented in this book.

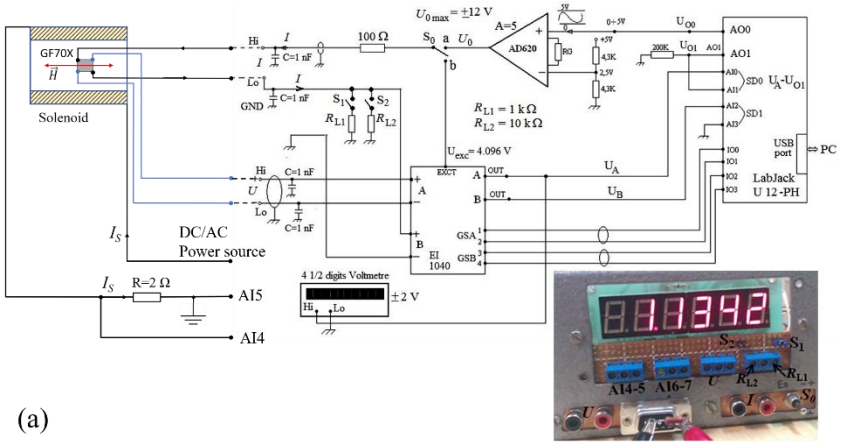

(a) (b)

Fig. 6. (a) Schematics of the experimental setup; dot lines signify connection leads between the chip with GMR sensors and the DAQ system. The settings used are: S_0 in position "b", S_1 closed, S_2 open; (b) Image of the mounted chip on a DIP-8 socket.

Using the settings described above, the GF70X (X=5 or 8) chip will be supplied with 4.096 V which assures a safe working regime. The supply current can be monitored by reading the voltage across R_{L1}=1 kΩ, which is applied to channel B of the instrumentation amplifier and then to AI2-AI3 from the DAQ board. The output voltage from GF70X sensor is applied to channel A of the instrumentation amplifier. The amplified signal is, then, applied on AI0-AI1 terminals of the DAQ board. The gain of the instrumentation amplifier can be set digitally from ports IO0-IO1 for channel A and IO2-IO3 for channel B, Fig. 6(a). A DC or very low

frequency AC power supply source is used to drive the current I_S through solenoid. If a DC source is used, a manual switch of the connection leads must be used in order to allow both positive and negative currents through solenoid. The current, I_S, generates a voltage across the resistor R=2 Ω. This voltage, applied to channels AI4-AI5 from DAQ, is a measure of the magnetic field inside the solenoid.

The field characteristic of the solenoid is $H=I_S(A)x120$ [Oe] or $\mu_0 H=B=I_S(A)x0.012$ [T].

The chip is mounted on a sample platform which is placed inside the solenoid. The sample platform allows both orientations of the chip regarding the applied field, α=0, 90°, see Fig. 5(a).

3. The experimental procedure

Using the experimental setup described in Section 2, the following steps are recommended:

f) Before connecting the DAQ board to computer verify that the following settings are applied: S_0 in position "b", S_1 closed, S_2 open. This means that a load resistor R=1 kΩ is used to read the current I. Connect the socket with the GF705 chip in the mounting pad such that α=0, see Fig. 5(a) and gently introduce the sample platform inside the coil;

g) Connect the measurement system to computer and launch the application LJlogger. Configure the channels as follows: SD0 as 0-1 Diff, SD1 as 2-3 Diff and SD2 as 4-5 Diff. First row reads the output voltage, in V, the second row reads the current through sensor, in mA, and the third row reads the voltage across the resistor R=2 Ω. For 1 in "Multiplier" field and 0 in "Offset" field, the reading from "Scaled Data" is identical with "Voltage" field;

h) In the field "Multiplier" for channel SD2, write the value of the constant which converts the data from "Voltage" into current (A) or magnetic field (Oe or T). If the multiplier is 0.5 then, in "Scaled Data", the reading represents the current I_S (A). If the multiplier equals 0.5*120, then, in "Scaled Data", the reading represents the field *H* in Oe. The same can be applied to express the field in T;

i) Chose the right gain for each channel of the instrumentation amplifier. This can be done by using the "IO Direction" and "IO State Write" check buttons from LJlogger interface;

j) Turn on the DC or AC programable source and scan the field between ± 100 Oe, i.e., ± 10 mT. During this test adjust in a convenient way the gains for channels A and B and the measurement domains for SD0, SD1 and SD2. Save the panel settings;

k) From the main interface of LJlogger, go to "Configure", set a name for the data file and chose that data will be written in the data file at every 0.5 s. Return to the main window interface;

l) Check the button "Write to file" and start to acquire data by scanning the field from ± 100 Oe at least two times in order to have full cycles of the applied field. When finished, uncheck the "Write to file" button.

m) Disconnect the DAQ board from computer, remove the sample platform from solenoid and insert the socket with the chip in the mounting pad such that α=90°;

n) Repeat the measurement by following the steps from b) to g);

o) Do the same with the sensor GF708;

p) Start the application SciDAVis or other convenient software product and import data. Find the sensor sensitivity for the linear region of the field dependence of the output voltage. See Fig. 5(d) and Fig. 6.

The plots should look like in Fig. 7(a) for GF705 and like in Fig. 7(b) for GF708.

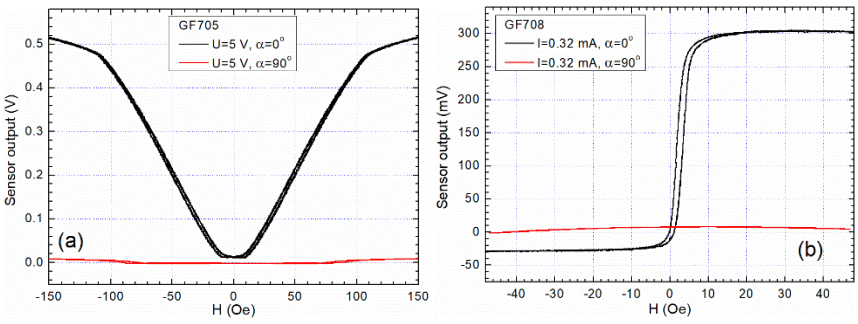

Fig. 7. The field characteristics of the output voltage for (a) GF705 and (b) GF708.

Discuss the using of GMR based magnetic sensors for practical applications like in automotive industry, brushless DC motors, magnetic media detection, etc.

VII. GMR based Non-contact Current sensor

1. Introduction and theoretical aspects

It is known that an electric curent, *I*, through a very long conductor generates a magnetic field expressed by:

$$H = \frac{I}{2\pi d} \text{ [A/m] or } B = \frac{\mu_0 I}{2\pi d} \text{ [T]} \quad (1)$$

as is illustrated in Fig. 1.

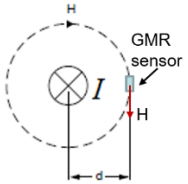

CURRENT (i)	DISTANCE (d)	MAGNETIC FIELD (H)	B (1 G=10^{-4} T)
10 mA	0.5 mm	3.18 A/m	3.99 10^{-6} T =0.0399 G
1 A	0.5 mm	318 A/m	3.99 10^{-4} T =3.99 G
1000 A	10 mm	15.9 kA/m	1.99 10^{-2} T =199 G

Fig. 1. The basic principle of current detection with a magnetic sensor

The magnetic field is detected using a sensor based on Giant Magnetoresistive effect (GMR) which is perfectly adapted to detect in plane magnetic fields, Fig.1.

The giant magnetoresistance (GMR) effect in thin-film multilayers was discovered separately in 1988 by Albert Fert, Baibich and coworkers at the Université Paris-Sud and by Peter Grünberg (Germany) on a Fe/Cr multilayer structure, Fig. 2. Fert and Grünberg were awarded with Nobel prize in Physics.

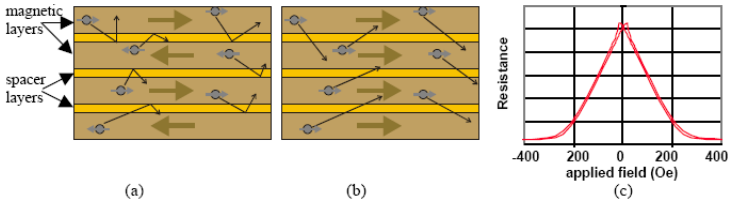

Fig. 2. Illustration of the GMR effect in magnetic multilayers: a) denotes the antiparallel (ap) state with a larger value of the structure resistance whereas b) shows the parallel (p) state configuration in magnetic layers with a smaller value of the structure resistance. The field dependence of GMR effect is presented in c).

The field dependence of the structure resistance can be expressed by:

$$R = R_0 + \frac{\Delta R_{GMR}}{2}(1 - \cos\theta) \quad (2)$$

where R_0 is the structure resistance at the saturated magnetic state; $\Delta R_{GMR}=R_{ap}-R_p$ is the amplitude of the GMR effect. θ is the angle between the magnetization directions from two adjacent layers which, in turn, depends on the magnetic field applied in the film plane. By using the freeware program Simulmag, one can study different types of magnetic multilayered thin films and simulate their GMR response in function of the applied magnetic field. Fig. 3 shows how is working the GMR based current sensor. The image is a snapshot taken during the simulation (see "Computer simulation of magnetization curves in magnetic thin films with Simulmag")

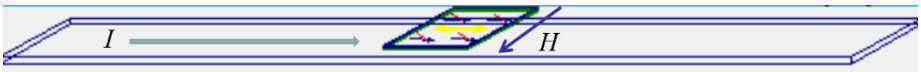

Fig. 3. The working principle of the GMR based current sensor. The red and blue arrows represent magnetizations from two adjacent magnetic layers.

The current, I, which is flowing through the conductive stripe generates a magnetic field, H, which can rotate the magnetization from the free layer (**red arrows**). The magnetic moments from the pinned layer (**blue arrows**) suffer only a small rotation. The sensor's resistance is changing due to the magnetic field generated by the current I. Based on this, an Ammeter with galvanic isolation can be built.

A practical implementation of a GMR based current sensor is represented schematically in Fig. 4.

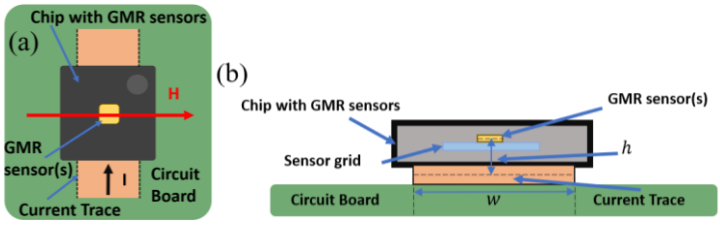

Fig. 4. Non-contact current measurement basic setup using a conducting trace and a GMR based sensor chip: (a) Plane view; (b) cross section. Image from https://doi.org/10.3390/s20010323

The current, I, from the conductive trace, named *current trace*, generates a magnetic field, whose component, B, parallel with the trace surface, is detected by the GMR sensor, Fig. 4. Usually, the trace thickness is between 0.018 to 0.036 mm and h is about 0.3 to 0.8 mm for low-profile surface mount packages chips, like TDFN. An analytical method, which assumes that the *sensor is centered above the trace* at distance h, Fig. 4, was developed [https://doi.org/10.3390/s20010323] to calculate B:

$$B = \left[\frac{I}{w} \cdot \arctan\left(\frac{w}{2h}\right)\right] \cdot 4 \cdot 10^{-7} \text{ [T]} \quad (3)$$

The results from equation (3) can be expressed in [G] by:

$$B = \left[\frac{I}{w} \cdot \arctan\left(\frac{w}{2h}\right)\right] \cdot 4 \cdot 10^{-3} \text{ [G]} \quad (4)$$

If h=0.345 mm (AAL024-10E produced by NVE - https://www.nve.com/analogSensors), w=1.25 mm and I=1 A, one finds B=3.42×10^{-4} T=3.42 G. Remember that in vacuum, air or other "nonmagnetic" materials, B(G) equals, numerically, H(G), i.e., μ_0=1 in C.G.S.em whereas $\mu_0=4\pi \cdot 10^{-7}$ N/A^2 in S.I.

In the linear region of the sensor's response, one can express the output voltage as:

$$\Delta U = S_B \cdot B = S_B \cdot K \cdot I = S_I \cdot I \quad (5)$$

where S_B is the effective field sensitivity which depends on the sensor type and supply voltage; $S_I=S_B \cdot K$ is the current sensitivity which, in addition, takes into account the sensing geometry, i.e., the values of w and h through the constant K – see the relation between B and I (eq. 3 and 4). A free app used to estimate the output voltage can be accessed at https://www.nve.com/spec/calculators#tabs-Current-Sensing. To increase the magnetic field generated by the current, I, the conductive trace can be replaced by a planar coil with n turns placed beneath the chip with GMR sensors, Fig. 5 - trace B. However, this can lead to an increase of the trace resistance and limits the applications for small currents detection. A method to calculate the magnetic field generated by a planar coil with n turns is presented in https://doi.org/10.3390/s21072564 .

2. The experimental setup

For experiments is used a Current sensor evaluation board, Fig. 5, which has three current measurement configurations A-C. Above of each current trace is placed a chip with GMR sensors.

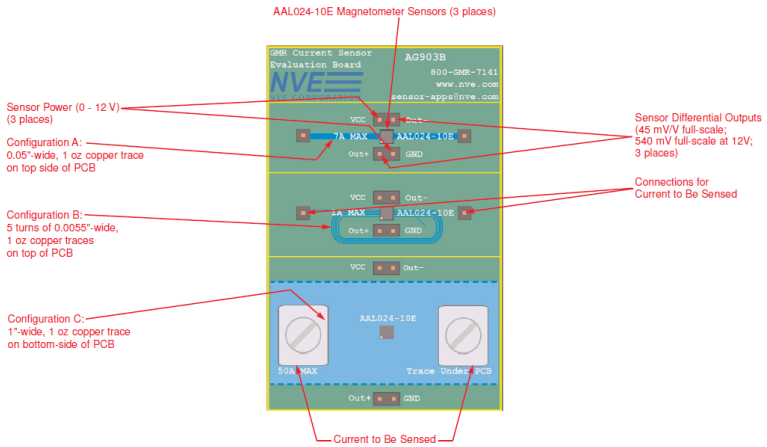

Configuration	Typical Sensitivity	Linear Range	Sensor Saturation	Isolation
A. Trace on top of PCB	8.6 mV/V/A	0 – 4.5 A	7 A	>300V
B. 5 turns on top of PCB	43 mV/V/A	0 – 0.75 A	1 A	>300V
C. Wide trace under PCB	0.9 mV/V/A	0 – 50 A	55 A	>6 kV

Fig. 5. Current sensor evaluation board and some typical characteristics (adapted from https://www.nve.com/EvaluationKits)

The chip, with GMR sensors used in these experiments, is AAL024-10E in TDFN package (2.5 mm x 2.5 mm) from NVE, Fig. 6. The main features are (https://www.nve.com/analogSensors):

- Wheatstone bridge configuration with 2 active GMR sensors and 2 GMR elements that are shielded and used to compensate the bridge at 0 field and to assure the thermal stability, 0.14 %/°C;
- Unipolar output characteristic, meaning the output voltage is positive for either field polarity i.e., the sensor detects only the absolute value of the magnetic field;
- Saturation magnetic field: 15 Oe (1.5 mT in air);
- Sensitivity: 3.6 mV/(V·Oe); linearity region: 1.5 to 10.5 Oe (i.e., 0.15 to 1.05 mT in air), see Fig. 6;
- *h*=0.345 mm (see Fig. 4);
- Typical bridge resistance (resistance between pins 1-4 and 3-6, respectively): 2.2 KΩ;
- Wide bandwidth, 500 kHz and low hysteresis, 2% max., for excellent repeatability.

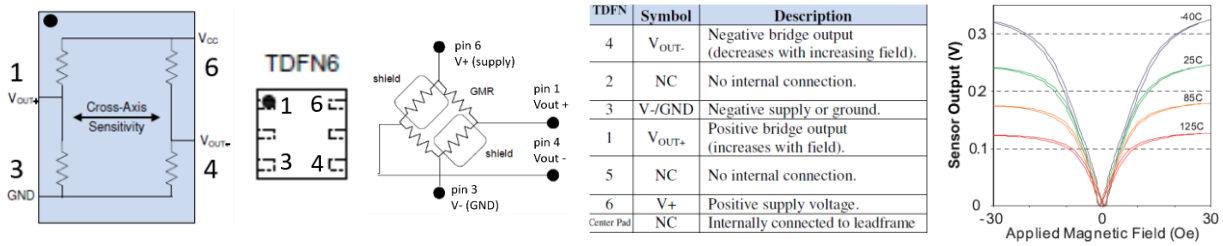

TDFN	Symbol	Description
4	V_{OUT-}	Negative bridge output (decreases with increasing field).
2	NC	No internal connection.
3	V-/GND	Negative supply or ground.
1	V_{OUT+}	Positive bridge output (increases with field).
5	NC	No internal connection.
6	V+	Positive supply voltage.
Center Pad	NC	Internally connected to leadframe

Fig. 6. The electrical schematics and pins configurations of AAL024-10E GMR based magnetic sensor from Nonvolatile electronics and some field characteristics when the supply voltage is 5 V.

A NI-ELVIS prototyping system will be used to drive the current through the desired trace (A or B) and to measure the output signal from the corresponding sensor. NI-ELVIS provides a breadboard where an electronic project can be developed and tested, a series of soft panel instruments like DMM, oscilloscope, variable power supply sources, signal analyzers, and others. In addition, an instrumentation amplifier EI 1040 and an ammeter will be used. This instrumentation amplifier converts the floating signal from GMR sensor into a single ended amplified signal. The gain will be 10. The connections will be made according to the notations from the testing board and the pins configuration, Figs. 5 and 7. The supply voltage for each sensor will be provided by EI 1040 (EXCT pin) and is set to 4.096 V. The schematics of GMR sensors' connections is presented in Fig. 7(a) and the electrical connection of the testing Trace (A or B) is presented in Fig. 7(b).

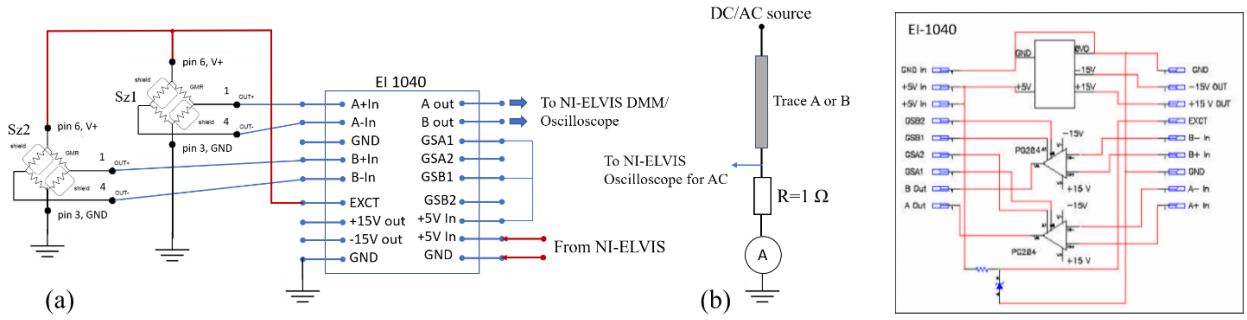

Fig. 7. Schematics of the experimental setup and the internal structure of the dual channel instrumentation amplifier EI-1040

3. The experimental procedure

The following main steps must be followed in order to characterize the current sensor:

a) The circuit corresponding to trace A, Fig. 5, will be connected to NI ELVIS. In addition, an ammeter will be connected in series with trace in order to read the applied current. When a DC current is applied through the conductive trace, the current is read by ammeter and the output voltage is read using the soft panel instrument "Digital Multimeter". When an AC current source is used, the ammeter is removed and the voltage across R is applied to channel A, whereas the voltage from EI-1040 is applied to channel B of an "oscilloscope" soft panel instrument.

b) Will be recorded U_{out} =f(I) in DC mode, I=f(t) and U_{out}=f(t) for AC currents taking care to **not exceed 1 A for trace A and 0.2 A for trace B**.

c) Data will be plotted both for DC and AC currents and conclusions will be drawn regarding the shape of the curves which are due to unipolar output field characteristic, Fig. 6. As expected results: (i) the output voltage

is positive for either current polarity and (ii) the GMR sensor produces an output analogous to half-wave rectification of the AC current being sensed, eliminating the need for rectification of AC inputs.
c) The sensitivity, S(mV/A), will be calculated for the linear region of the characteristics.
d) The steps from b-c will be repeated for trace B. The obtained sensitivities will be compared with data from table presented in Fig.5.

These experiments will be repeated when an external biasing field of about 5 Oe is applied along the "Cross-axis sensitivity". For this purpose, an external magnet will be properly positioned in the vicinity of the evaluation board to polarize the sensor. By this, the sensor's output, for I=0, will be situated in the linear region of the field characteristic, Fig. 6. This will be taken as the new bridge offset that can be compensated to 0. In other words, the sensor output for different values of current will be measured *relative* to this new offset value. Conclusions regarding linearity and current sensitivity, when the sensor is biased, will be drawn. Compare the sensitivities for traces A and B.

Discuss the using of GMR sensors for current sensing applications highlighting the pros and cons compared with other methods.

VIII. Angle magnetic microsensor

1. Introduction and theoretical aspects

When a rotating magnetic field is applied in the plane of a giant magnetoresistance sensor (GMR), the output voltage follows a sine or cosine dependence on the angle between the axis of maximum sensitivity of the sensor and the direction of the applied field.

The GMR effect in thin-film multilayers was discovered separately in 1988 by Albert Fert, Baibich and coworkers at the Université Paris-Sud and by Peter Grünberg (Germany) on a Fe/Cr multilayer structure, Fig. 1. Fert and Grünberg were awarded with Nobel prize in Physics. More discussion about the GMR effect was done at the introduction of "Magnetic field microsensors based on GMR effect" work.

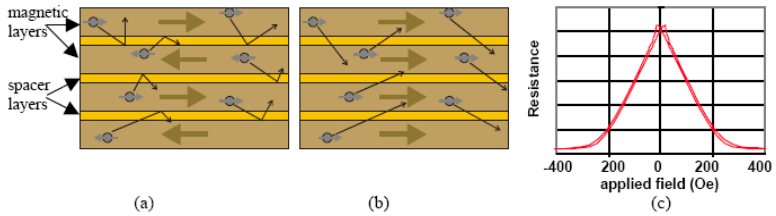

Fig. 1. Illustration of the GMR effect in magnetic multilayers: a) denotes the antiparallel (ap) state with a larger value of the structure resistance whereas, R_{ap}; b) shows the parallel (p) state configuration in magnetic layers with a smaller value of the structure resistance, R_p. The field dependence of the GMR effect is presented in c).

The field dependence of the structure's resistance can be expressed by:

$$R = R_0 + \frac{\Delta R_{GMR}}{2}\left(1 - \cos\theta\right) \qquad (1)$$

where R_0 is the structure resistance at the saturated state; $\Delta R_{GMR}=R_{ap}- R_p$ is the amplitude of the GMR effect. θ is the angle between the magnetization directions from two adjacent layers which, in turn, *depends on the magnetic field, applied in the film plane*. By using the freeware program, Simulmag, one can study different types of magnetic multilayered thin films and simulate their GMR response in function of the applied magnetic field. The simulated GMR structure is presented in Fig. 3 and consists from an exchange biased trilayer. The magnetization from one magnetic layer (blue arrows) is pinned through exchange interaction, H_{pin}=200 Oe, whereas the magnetization from the sensing layer (red arrows) is free to rotate. Between the magnetic layers there is a positive coupling described by H_{coupl}=70 Oe – see the practical work devoted to micromagnetic simulations on thin magnetic layers.

Micromagnetic simulations and experimental data show a dependence of the field dependence of the GMR effect on the angle between the anisotropy axis and the applied magnetic field. These results are presented in Fig. 2.

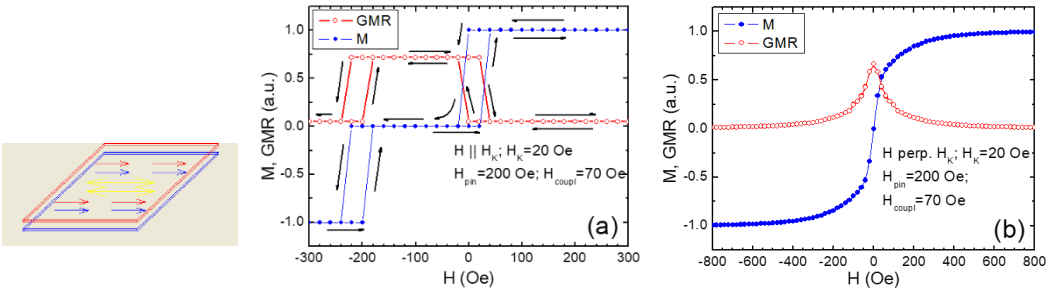

Fig. 2. Micromagnetic simulations with *SimulMag* for magnetization curves and GMR curves when H is applied (a) along the easy axis and (b) perpendicular un the easy axis; with yellow arrows is shown, on the simulated structure, the anisotropy axis.

These simulations suggest that an angular dependence of the output signal may appear when a constant magnetic field rotates in the sensor's plane. This behavior is illustrated through micromagnetic simulations in Fig. 3. The simulated GMR structure is presented in Fig. 3(a) and consists from an exchange biased trilayer.

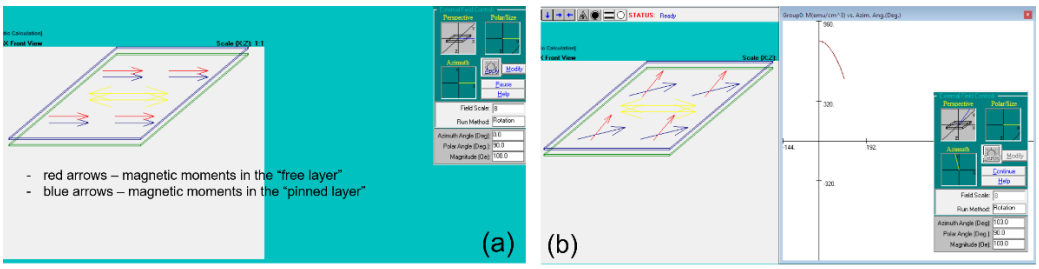

Fig. 3. (a) The simulated GMR structure and (b) the magnetic moments orientation in both magnetic layers and the angular dependence of the total magnetization when the applied field, H, is rotated in the film plane (xoy plane); here H=100 Oe

Fig. 4 shows the angular dependence of the structure magnetization and of the GMR effect found by micromagnetic simulations on the structure depicted in Fig. 3. More about micromagnetic simulations using Simulmag can be found in „Computer simulation of magnetization curves in magnetic thin films with Simulmag". The shape of these curves can be adjusted to follow more acurately a sine function by changing the structure and shape of magnetic sensors through microfabrication processes.

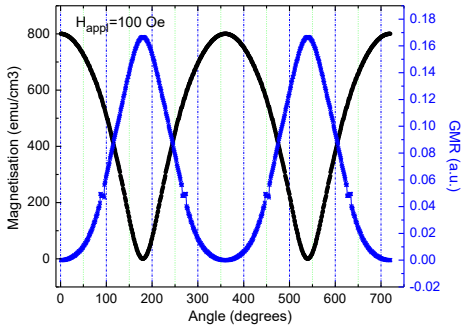

Fig. 4. The angular dependence of the structure magnetization and of the GMR effect.

The main features of the angular dependence of the GMR effect in such structure are: (i) there is a sine or cosine dependence of the GMR effect and (b) for one complete rotation of the magnetic field, the GMR effect shows two periods. These properties suggest that a GMR field sensor can be used, also, as a rotation sensor.

2. The experimental setup

To study the rotation sensor is used an evaluation board from Nonvolatile electronics (NVE), Fig. 5. This board consists from a chip with 4 Tunnelling Magnetoresistance (TMR) sensors, which makes an angle of 90° between them such that for one pair of sensors a signal in $\sin\theta$ is obtained whereas for the second pair, a signal in $\cos\theta$ results; θ is the rotation angle of the field. The field, parallel to the sensor surface is generated by a split-pole cylindrical magnet which can rotate above the sensor. Two operational amplifiers are used as buffers (gain 1) to adapt the high output impedance of the TMR sensors with the measurement electronics. The TMR sensor has a structure quite similar to that of a GMR sensor except the nonmagnetic layer which is an oxide like Al_2O_3 or MgO_2 instead of Cu. The current flows perpendicular to the sensor surface by tunnelling effect. When the magnetizations from the magnetic layers are parallel, the tunnelling probability is larger and structure's resistance is smaller. When the magnetizations are antiparallel, the tunnelling probability is smaller and structure's resistance is smaller. So, the field behavior of the TMR effect is very similar to that of the GMR effect but the amplitude of the TMR effect is at least 10 times larger.

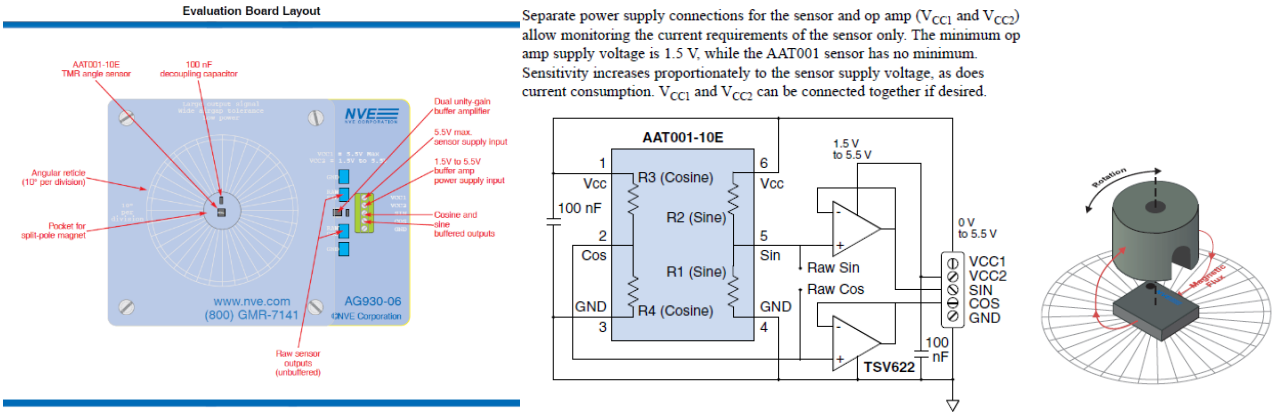

Fig. 5. The evaluation board, layout and his schematics, used to study the rotation sensor; the magnet is shown as well.

3. The experimental procedure

a) Connect V_{CC1} and V_{CC2} to a DC variable power supply source; adjust the supply voltage for V_{CC1} and V_{CC2} according to instruction from Fig. 5. For example, one can start with V_{CC1}=3 V and V_{CC2}=4 V;
b) Connect the "sin" and 'cos" screw terminals to an oscilloscope or to two digital voltmeters;
c) Place the split-pole magnet, attached to a digital protractor, in the Plexiglas pocket SLOT DOWN (see Fig. 5);
d) Rotate the magnet until a maximum value is measured on the "cos" output. This means that θ=0;
e) From this position, start to rotate the magnet from 5 to 5 degrees and record the sensor's signal both for sin and cos outputs;
f) Represent on the same plot the angular dependences of the signals from sin and cos outputs;
g) Repeat the measurements for other supply voltages V_{CC1} and V_{CC2}; do not overpass 5 V and keep V_{CC2}>V_{CC2};
h) Find the sensitivity of the sensors expressed in V/degree in the linear region of the output characteristics.

The outputs should be similar to the graph from Fig. 6:

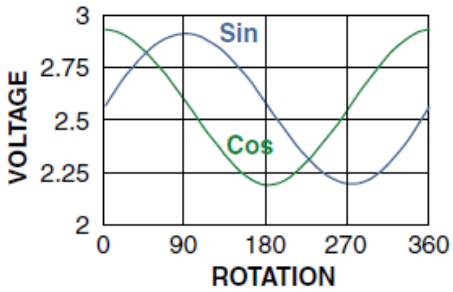

Fig. 6. Example of the sensor outputs

Additional tasks:

Discuss the using of rotation sensors for practical applications like in automotive industry, brushless DC motors, etc.

Take two DVMs and connect one voltmeter between "Raw Sin" and Ground and the second voltmeter between "Sin" and Ground outputs, Fig. 5. See the readings and discuss the importance/role of the operational amplifiers. Do the same for "Raw Cos" and "Cos" outputs.

IX. Study of photoconductivity- photoresistors

1. Introduction

Photoconductivity (PC) consists in changing of electrical conductivity of a semiconductive material due to the absorption of electromagnetic (e.m.) radiation such as visible light, ultraviolet light, infrared light, or gamma radiation. When light is absorbed by a semiconductor, the number of *free electrons* and *holes* increases, resulting in *increased electrical conductivity*. To cause this behaviour, the *photons*, i.e., the particles associated with e.m. radiation that strikes the semiconductor, must have enough energy to raise electrons across the band gap, or to excite the impurities within the band gap. Note that the energy of one photon is $E_{photon} = hv$ where $h = 6.626\times10^{-34}$ J/s is the Planck's constant whereas v is the frequency of e.m. radiation. Such that, if the frequency is smaller than a threshold value, the photons will have an energy smaller than the bandgap and the generation of free electrons (in conduction band) and free holes and the electrical conductivity is not changing regardless the intensity of the e.m. wave. The height of the bandgap depends on the material properties through the type semiconductor like Si, Ge, GaAs, etc. and on doping atoms like P, Al, B and so on. It comes that this effect is not seen in metals where the concentration of electrons, that can move freely inside, is not affected by the applied e.m. radiation. In many semiconductors the absorption of electromagnetic radiation can show a frequency selectivity as well. Fig. 1 illustrates this effect.

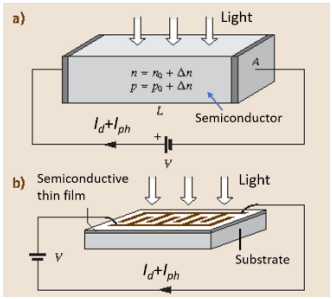

Fig. 1. (a) Schematic illustration of photoconductivity in semiconductors and (b) the using of this effect to build a *light-dependent resistor* (LDR) or simply *photoresistor* (adapted from https://doi.org/10.1007/978-3-319-48933-9_7); I_d is the dark current (no applied light) and I_{ph} is the current due to generation of supplementary charges Δn and Δp when light is applied. n_0 and p_0 represent concentration of charges in semiconductor at dark. Note that usually $I_d << I_{ph}$.

When a bias voltage and a load resistor are used in series with the semiconductor, a change of the voltage drop across the load resistors can be measured as a measure of the change in electrical conductivity of the material due to applied light. Based on this effect are build the LDR sensors. Most semiconductors used to build LDRs are sensitive in IR and visible radiation.

2. Theoretical aspects

a. Charge generation

When light, with frequency larger than the threshold value, is applied to a semiconductor, the concentration of electrons and holes that can contribute to conduction becomes:

$$\begin{aligned} n &= n_0 + \Delta n \\ p &= p_0 + \Delta p \end{aligned} \qquad (1)$$

where n_0 and p_0 are concentrations of carriers (electrons and holes) at equilibrium in dark whereas Δn and Δp represent nonequilibrium concentrations of carriers due to applied e.m. radiation.

Electrical conductivity due to applied light is:

$$\sigma = \sigma_0 + \Delta\sigma \qquad (2)$$

where

$$\sigma_0 = q\left(\mu_n n_0 + \mu_p p_0\right) \qquad (3)$$

is conductivity at dark and

$$\Delta\sigma = q\left(\mu_n \Delta n + \mu_p \Delta p\right) \tag{4}$$

is nonequilibrium conductivity due to applied light.

When light is applied, Δn and Δp start to increase until a steady state is established, described by Δn_{st} and Δp_{st}, see Fig. 2(a). This stabilization is due to the interplay between generation and recombination of free charges (electrons and holes). Hence, after a specific time the concentrations of free carriers that can contribute to conduction will reach stationary values under constant intensity of the applied e.m. radiation – in particular I.R. or visible radiation. We must note that the magnitude of Δn_{st} and Δp_{st} depends on the light intensity, i.e., on the number of photons/(m^2×s) that reach the surface of the semiconductor.

For stationary concentration of nonequilibrium electrons extracted from valence band (V.B.) to conduction band (C.B.) can be used the expression:

$$\Delta n_{st} = \alpha\beta I_r \tau_n = g\tau_n \tag{5}$$

where: α - absorption coefficient of light;

β - quantum efficiency of charge extraction from V.B. to C.B.;

I_r – intensity of the incident radiation;

τ_n - mean life time of electrons in C.B.

$g = \alpha\beta I_r$ – optical rate generation of electrons.

Similar relations can be found for holes generated due to light:

$$\Delta p_{st} = \alpha\beta I_r \tau_p = g\tau_p \tag{6}$$

Such that, we can express the steady state value of the conductivity change due to optical generated carriers:

$$\Delta\sigma_{st} = qg\left(\mu_n \tau_n + \mu_p \tau_p\right) \tag{7}$$

If there is a conduction based on a majority type of carriers, e.g., electrons, we have a so-called monopolar photoconductivity described by:

$$\Delta\sigma_{st} = qg\mu\tau \tag{8}$$

b. Relaxation of photoconductivity

We suppose that at t=0 the light with constant intensity is applied to semiconductor. Because of the concurrent generation-recombination processes the conductivity reaches a steady state value after a definite time. When light is turned off, Δn is not going to zero instantaneously. There is a finite time needed for recombination of the nonequilibrium carriers (electrons and holes), Fig. 2(a). As a consequence, a tail will appear in the time dependence of the current, I_{ph}, due to charges generated by light excitation. Such behaviour has implications when photoresistors are used to detect light that has a rapid time variation.

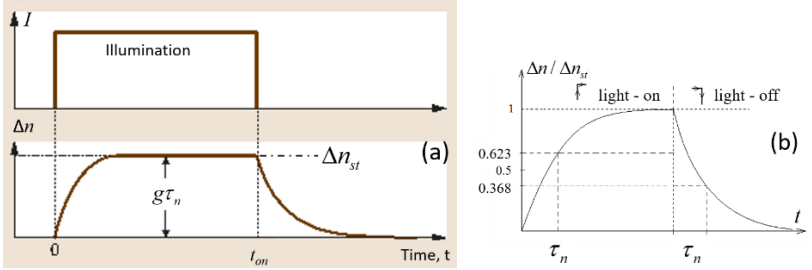

Fig. 2. (a) Illustration of time dependence of Δn when the incident light is on/off (adapted from https://doi.org/10.1007/978-3-319-48933-9_7) and (b) details explaining the time dependence of the nonequilibrium charge carriers generated by optical excitation and the meaning of τ_n.

For simplicity, we consider small injection levels (and linear recombination processes) which are established for low light intensity and semiconductors with small band gap and temperatures larger than 273 K, i.e., large values for n_0 and p_0. In this case, $\Delta n << n_0+p_0$. From initial condition $\Delta n(0)=0$, we find:

$$\Delta n = g\tau_n\left(1-e^{-\frac{t}{\tau_n}}\right) \tag{9}$$

and, for $t\to\infty$, $\Delta n_{st} = g\tau_n$, Fig. 2.

When light is turned off at a moment that can be referred as t=0, we can now consider as initial condition, $\Delta n\big|_{t=0} = \Delta n_{st}$ and we find:

$$\Delta n = g\tau_n \exp\left(-\frac{t}{\tau_n}\right) \tag{10}$$

From equations 9 and 10 we can plot the relaxation curves for increasing and decreasing of photoconductivity, Fig. 2(b).

c. Characterization of photoconductivity from experimental data

The circuit that can be used to characterize the photoconductivity in a semiconductor is presented in Fig. 3. The photoresistor is connected in series with a load resistor, R_L, to a source of voltage V.

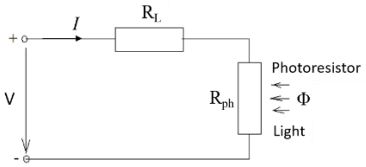

Fig. 3. Simplified schematic of the circuit used the characterize the photoconductivity

We suppose that the semiconductor sample has a resistance R_d at dark which decreases with ΔR to R_{ph} when light is applied: $R_{ph} = R_d - \Delta R$.

If the current through the semiconductive sample is I_d at dark and I_{ph} when light is applied, the signal on the load resistance due to applied light is

$$V_{ph} = R_L\left(I_{ph} - I_d\right) \tag{11}$$

and we can express the variation of the sample resistance due to light by:

$$\Delta R = \frac{\left(R_L + R_d\right)^2 V_{ph}}{V\cdot R_L + V_{ph}\left(R_L + R_d\right)} \tag{12}$$

Variation of the sample conductivity is:

$$\Delta\sigma_{ph} = \sigma_{ph} - \sigma_d = \frac{l}{S}\left(\frac{1}{R_{ph}} - \frac{1}{R_d}\right) = \sigma_d\,\frac{\Delta R}{R_d - \Delta R} \tag{13}$$

where l is the length and S represents the cross-section area of the sample.

For simplicity, we can consider two extreme situations:

i) $R_L << R_d$ (constant electric field regime)
As $V_{ph}<<V$, we get:

$$\Delta\sigma_{ph} = \sigma_d \frac{R_d}{R_L} \cdot \frac{V_{ph}}{V} \tag{14}$$

ii) $R_L >> R_d$ (constant current regime)

$$\Delta\sigma_{ph} = \sigma_d \frac{R_L V_{ph}}{V R_d - V_{ph} R_L} \tag{15}$$

Because it is difficult to know the sample's geometrical parameters, it is much more useful to express the relative variation of the conductivity.

For constant electric field regime, $R_L << R_d$ we have:

$$\frac{\Delta\sigma_{ph}}{\sigma_d} = \frac{R_d}{R_L} \cdot \frac{V_{ph}}{V} \tag{16}$$

whereas, for constant current regime $R_L >> R_d$ we have:

$$\frac{\Delta\sigma_{ph}}{\sigma_d} = \frac{R_L V_{ph}}{V R_d - V_{ph} R_L} \tag{17}$$

In general, the dependence of photoconductivity on the incident luminous flux, Φ, is of the type

$$\Delta\sigma_{ph} = A \cdot \Phi_0^{\gamma} \tag{18}$$

where A is a material constant and γ is a nonlinearity energetic coefficient of photoconductivity.

For linear recombination, γ =1, increasing and decreasing of photoconductivity has an exponential behaviour, described by equations 9 and 10, and characterized by the same time constant – mean life time of the nonequilibrium carriers. Instead, for quadratic recombination γ = ½, life time of the nonequilibrium carriers decreases with the increases of the flux of light.

d. I-V characteristics of a photoresistor

When the applied voltage on PR is V_{PR}, the I-V dependence is:

$$I_{PR} = I_d + I_{ph} = C_0 \cdot V_{PR} + C_f \cdot \Phi^{\gamma} \cdot V_{PR} \tag{19}$$

where I_d and I_{ph} are the currents at dark and when light is applied; C_d and C_{ph} are material constants.

It comes from eq. 19 that dependences I_{PR}=f(V_{PR}) are linear with slopes which depend on the flux of the applied light.

3. The experimental setup

The main schematics of the experimental setup is presented in Fig. 4. It consists from two parts: (i) the circuit that generates the applied light on the PR (left hand part) and (ii) the circuit used to characterize the photoresistor.

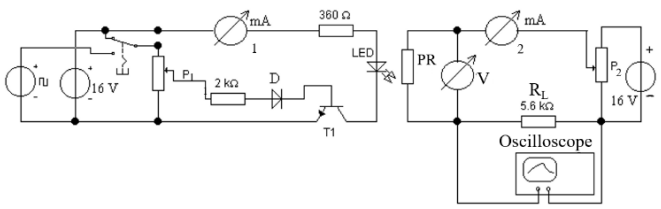

Fig. 4. The schematics of the experimental setup

The light is emitted by a red LED because for such device we can assume that $\Phi \sim I_{LED}$. The driving circuit can apply both DC and current pulses which can be controlled by a potentiometer P_1 and transistor T_1. To apply current pulses through LED, a function generator is used to send square wave pulses to the base junction of the transistor T_1. The circuit used to characterize the photoresistor has a typical schematic for an I-V characterization system. The voltmeter needs to have a very large input resistance to avoid shunting effects when the PR is at dark. In addition, a two channels digital oscilloscope is connected on the load resistor in order to visualize the time dependence of the current when light pulses are applied on PR. The second channel is connected to the output of the function generator. Such that, curves like in Fig. 2 can be plotted; note that the measured voltage on the load resistor is proportional to the current I_{PR} which, in turns, is proportional with the charge density n. The practical implementation of the schematics from Fig. 4 implies, the using of conventional digital meters (ammeters and voltmeters), DC sources and a NI-ELVIS device that brings the flexibility of soft panel (SFP) instruments like oscilloscope, function generator and two wire characterization facility. The LED and the PR are placed inside of an opaque tube in order to avoid perturbations due to external light.

4. The experimental procedure

4.1. Static characterization

The PR is connected to a NI-ELVIS breadboard and is launched the "Two wire current-voltage analyzer" SFP. The LED is supplied with a DC current, using the schematic depicted in Fig. 4.

The following experimental steps are recommended:

q) For I_{LED}=0 (dark) is raised the I_{PR}=f(V_{PR}) characteristic. The voltage is varied between ±10 V with an increment of 0.5 V; in this case, the measured current represents I_d (see eq. 19). The generated data file will be saved;

r) The same experiment will be run for I_{LED}= 2, 4, 6 and 8 mA i.e., different values of the applied flux of light. The measured current will be $I_{PR}=I_d+I_{ph}$. Data will be saved again for each value of I_{LED}. Compare the I_{PR}=f(V_{PR}) characteristics with the results recorded at dark;

s) The characteristics I_{PR}=f(V_{PR}), for I_{LED}=0, 2, 4, 6, and 8 mA will be plotted. Using linear fitting will be obtained the slopes of these plots for each value of I_{LED}. These slopes represent the conductance of the PR at dark, G_d, and for different illuminations, G. The resistance of the PR can be calculated with $R_d=1/G_d$ at dark and $R=1/G$ for different illuminations. Now, R_d can be compared with R_L to confirm the constant field polarization regime (see section 2.c). The values of R_d and R for different values of I_{LED} will be marked on the corresponding plots;

t) Using data acquired in previous experiments (a, b), we can choose two voltages V_{PR} e.g., 4 and 8 V for which can be calculated the photocurrent due to nonequilibrium carriers: $I_{ph}=I_{PR}-I_d$. By plotting I_{ph}=f(I_{LED}) for V_{PR}=4 and 8 V, can be estimated γ, i.e., the coefficient of photoconductivity and hence the recombination mechanism. If I_{ph}=f(I_{LED}) has a linear dependence, γ=1. If I_{ph}=f(I_{LED}) has a quadratic dependence, i.e., can be fitted with a second order function, then γ=1/2.

4.2. Dynamic characterization

For the next experiments, square wave pulses of currents will be applied through LED, Fig. 4. Two SFP instruments will be used: Function generator and the Oscilloscope. Channel 1 of the oscilloscope will be connected to the output of the Function generator whereas the second channel will be connected on R_L to give the wave form of the photocurrent. To visualize the signal due only to I_{ph}, the coupling for channel 2 will be set to AC. By this, the DC component of the current, corresponding to I_d, will be canceled. The working frequency is in the range of a few Hz.

The following experimental steps are recommended:

d) The supply voltage for PR is set to 6 V. By tunning the amplitude and the frequency of the function generator, dependences like in Fig. 2(a) can be visualized on the Oscilloscope SFP instrument. By using the details described in Fig. 2(b), can be calculated the mean life time of carriers τ.

e) The steps from (a) can be repeated for other values of V_{PR} and frequencies of the square shaped current through LED for which stable images can be obtained on oscilloscope. A mean value of τ will be expressed after these measurements;

f) The frequency of the square shaped current through LED will be increased until the plateau from Fig. 2(a) for I_{ph} disappear. Can be seen a relation between the period of this current and τ?

Fig. 5 presents a simple implementation of a LDR using an Arduino uno board.

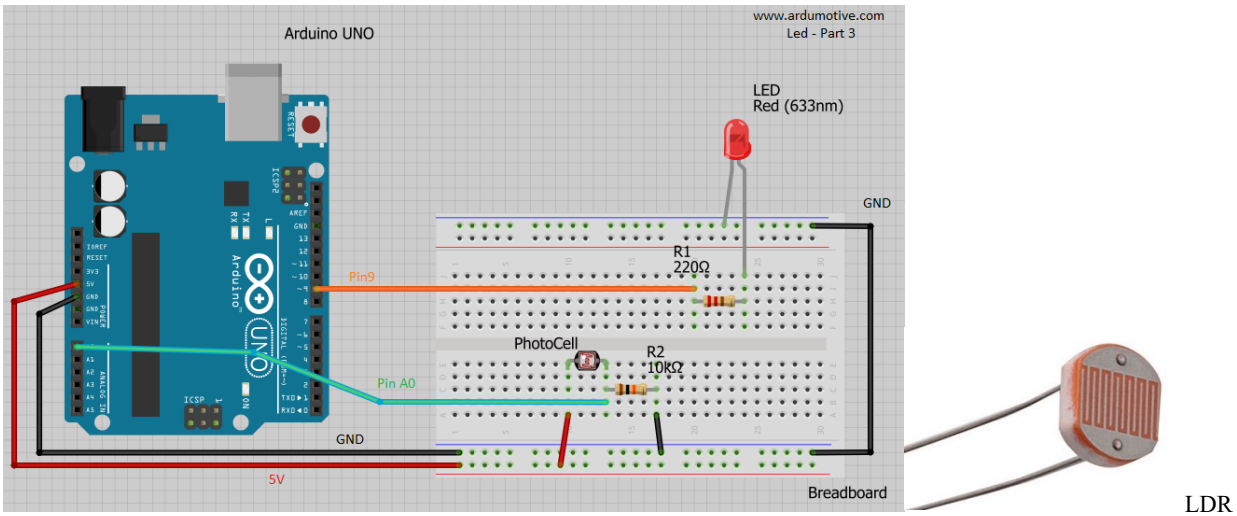

Fig. 5. Practical implementation of a LDR using an Arduino uno board and a photoresistor (image from https://www.instructables.com/How-to-use-a-photoresistor-or-photocell-Arduino-Tu/)

Additional tasks:

1. Give a brief discussion on the possible applications of the photoconductivity.
2. Implement this schematic in https://wokwi.com/ and test the code needed to run a light detection device.
3. Discuss the differences between a photoresistor and a photodiode.
4. Can you design a differential ligth detector with PR able to compensate the temperature variation of the sensor's resistance?

X. Study of the photodiode

1. Introduction

Photodiode (PD) is a light-sensitive semiconductor diode whose junction is exposed to electromagnetic radiation, in particular light (or infrared, ultraviolet radiation, or X-rays). The package of a PD may include lenses or optical filters to increase his sensitivity and spectral selectivity. Devices designed for use as a photodiode use a PIN junction rather than a p–n junction, to increase the speed of response. A photodiode is designed to operate in *reverse bias*, i.e., positive potential applied on cathode and negative potential applied to anode, and has a spectral sensitivity which depends on the semiconductive materials used for fabrication. Such that, the PDs made from Silicone can detect radiation with a wave length range between 190 to 1100 nm whereas Indium gallium arsenide PDs can detect radiation with wave length ranging between 800 to 2600 nm.

2. Theoretical aspects

Photodiode is a p-n junction, as depicted in Fig. 1. When a photon, with a high enough energy, strikes the p-n junction, it creates an electron–hole pair, see section IX. This is known as the *inner photoelectric effect*. If the absorption occurs in the junction's depletion region, or one diffusion length, $L_{n,p}$, away from it, these carriers are swept from the junction by the built-in electric field, $\vec{E}_i$, of the depletion region, Fig. 1(a and c). Such that, holes move toward the anode which becomes positively charged, and electrons toward the cathode. An open circuit voltage is measured if K is open and a photocurrent is produced when K is closed. The charge accumulation continues until a steady state is found due to the competition between the field generated by the nonequilibrium charges and the internal field. By a consequence, the built-in electric field ($\vec{E}_i$) decreases and the width of the depletion region decreases as in the case of a forward applied voltage. Now, if a reversed biased voltage is applied, the total current through the photodiode is the sum of the dark current (current that is generated in the absence of light) and the photocurrent; so, the dark current must be minimized to maximize the sensitivity of the device.

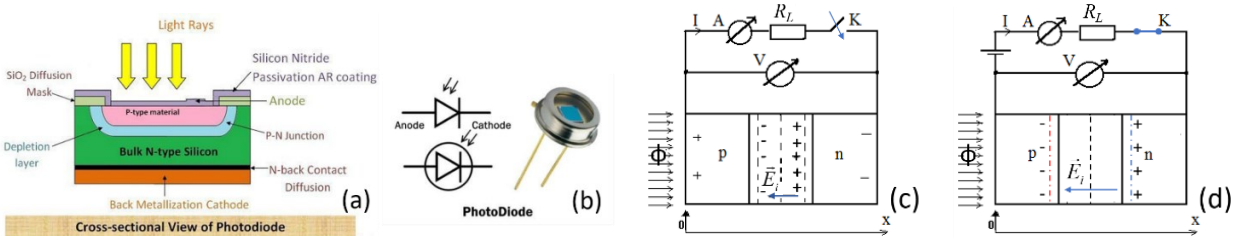

Fig. (a) Structure of a photodiode in a cross-sectional view (adapted from https://electronicscoach.com/photodiode.html) and (b) the symbol of photodiode. A simple characterization circuit is presented in (c) and (d).

For a given spectral distribution, the photocurrent is linearly proportional to the irradiance or simply the light intensity (the flux of light received by a surface per unit area).

Two basic modes can be found for photodiodes.

i. Photovoltaic mode – zero bias

The photovoltaic mode occurs with zero bias, i.e., no external source is connected, Fig. 1(c). The photocurrent flows from the anode (p region) through a short circuit to the cathode (n region). If the circuit is opened (K – open) or has a large load impedance, restricting the photocurrent out of the device, a voltage builds up in the direction that forward biases the diode, that is, *anode positive with respect to cathode*. This is referred as *open-circuit voltage*, V_{OC}, and depends on the light intensity and junction structure. If the circuit is shorted (K – closed) or the connected impedance is very low, a forward current, named *short-circuit current,* I_{SC}, will consume all or some of the photocurrent. This mode exploits the photovoltaic effect, which is the basis

for solar cells – a traditional solar cell is just a large area photodiode. If R_L takes values from 0 to infinity, can be drawn the generation characteristic curve of the PD as seen in Fig. 2.

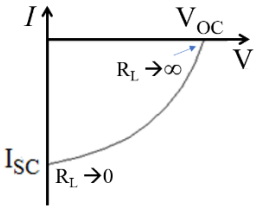

Fig. 2. The characteristic curve of the PD in photovoltaic mode.

It can be shown that exists a unique value of the load resistor, R_L=R_m, for which the power delivered by the PD is maximum.

ii. Photoconductive mode – reverse biasing

In photoconductive mode, the diode is reverse biased, i.e., with the cathode driven positive with respect to the anode, Fig. 1(d). This setup reduces the response time because the additional reverse bias increases the width of the depletion layer, which decreases the junction's capacitance and increases the region with an electric field that will cause electrons to be quickly collected. The reverse bias also creates dark current without much change in the photocurrent. Although this mode is faster, the photoconductive mode can exhibit more electronic noise due to dark current or avalanche effects. The leakage current of a good PIN diode is so low (<1 nA) that the Johnson–Nyquist noise of the load resistance in a typical circuit often dominates.

Neglecting recombination-generation effects in depletion layer, the characteristic equation given by Shockley theory is:

$$I = -I_L + I_S\left(e^{\frac{qV}{KT}} - 1\right) \tag{1}$$

where V is the applied voltage on PD, I_L is the current due to the applied light, independent on V, and I_S is the saturation current due to minority charges (typical for p-n junctions).

Based on equation 1 and experimental data, the following families of I-V characteristics for different levels of irradiance (i.e., the radiant flux received by a surface per unit area) can be plotted as in Fig. 3. These plots have mostly a qualitative character. The zone marked with (i) represents the photovoltaic mode whereas the zone marked with (ii) represents the photoconductive mode.

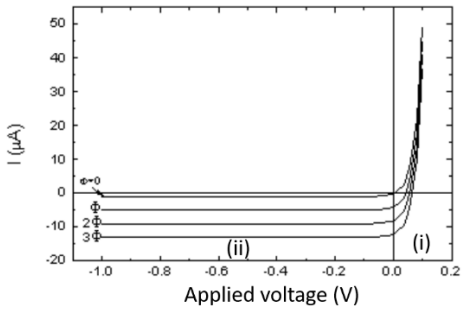

Fig. 3. Families of I-V characteristics based on eq. 1 and the assumption that $I_L \sim \Phi$

From equation 1, can be expressed the open circuit voltage and the short-circuit current by:

$$V_{OC} = \frac{KT}{q}\cdot\ln\left(1+\frac{I_L}{I_S}\right) \qquad I_{SC} = -I_L \tag{2}$$

3. The experimental setup

Fig. 4 presents the schematics of the experimental setup (see also section IX). The system consists from two parts: a typical I-V characterization setup for the p-n junction (left hand part) and a circuit with a controlled variable supply source that drives a current through LED (right hand part). The intensity of the light emitted by the LED is proportional with the current that flows through him, I_{LED}. The PD and LED are sealed inside of a black tube in order to prevent light from exterior. Voltmeter must have a very large input impedance,

of at least 100 MΩ, in order to avoid shunting effects. Note that a reverse biased PD presents a very high resistance.

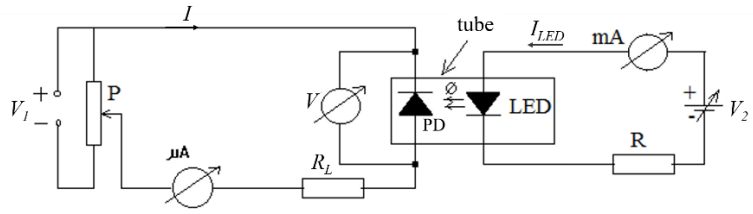

Fig. 4. Schematics of the experimental setup.

As described in Section IX – Study of photoconductivity, some of the measurement devices and sources, depicted in Fig. 4, can be replaced by soft panel instruments (SFP) from a NI-ELVIS prototyping board.

4. The experimental procedure

The following experimental steps are recommended:

a) The characterization circuit presented in Fig. 4 can be implemented using both standalone devices and SFP instruments from NI-ELVIS;
b) For I_{LED}=0 (dark), 4 mA, 8 mA, 12 mA and 20 mA will be measured the I=f(V) dependences by applying the following voltages on PD: 0, -0,05 V, -0,1 V, -0,15 V, -0.2 V, -0,4 V, -0,6 V, -1V, -2 V;
c) In open circuit regime (the microammeter is disconnected) will be measured the open circuit voltages, V_{OC}, generated by the PD for I_{LED}=0, 4 mA, 8 mA, 12 mA and 20 mA;
d) The acquired data can be recorded in the table below. According to equations 1 and 2, I_{SC}=-I_L when V=0;
e) Now, can be plotted the dependences I=f(V) for I_{LED}=0, 4 mA, 8 mA, 12 mA and 20 mA like in Fig. 3;
f) Also, will be represented, on the same plot, the dependences V_{OC}=f(I_{LED}) and I_{SC}=f(I_{LED});
g) Find which is the best detection regime: open circuit regime (V_{OC}) or short circuit regime (I_{SC})?
h) For the selected detection regime, discuss the associated conditioning circuit;
i) Discuss some applications of the photodiodes and present the main differences between photodiodes and phototransistors.

Suggested data table

I_{LED}	V (voltage on PD)	I (current through PD)	V_{OC}	I_{SC}
mA	V	μA	V	μA

Additional tasks

1. Remove the measurement instruments (voltmeter and ammeters). The source V_2 is now replaced by a SFP instrument "Function generator" from NI-ELVIS which is set to deliver square wave signals. Channel A of the oscilloscope from NI-ELVIS will be connected to the output of the Function generator. Channel B will be connected (i) directly on PD to measure the time dependence of V_{OC} (in open circuit regime) or (ii) on the load resistor to measure the time dependence of the current through PD for different polarization regimes. Run measurements and compare data with similar measurements made on photoresistors.
2. Can you implement and test in https://wokwi.com/ a light detector with photodiode using Arduino board?

Annex 1

International System of Units (Système Internationale d'Unités - SI)

Quantity	Name	Symbol
SI Base Units		
Length	meter	m
Mass	kilogram	kg
Time	second	s
Electric current	ampere	A
Temperature	kelvin	K
Amount of substance	mole	mol
SI Derived Units with Special Names		
Frequency	Hertz	Hz (s^{-1})
Force	Newton	N ($kg \cdot m/s^2$)
Pressure	Pascal	Pa (N/m^2)
Energy, work	Joule	J ($N \cdot m$)
Power	Watt	W (J/s)
Electric charge	Coulomb	C ($A \cdot s$)
Electric potential	Volt	V (W/A)
Capacitance	Farad	F (C/V)
Electric resistance	Ohm	Ω (V/A)
Conductance	Siemens	S (A/V)
Magnetic flux	Weber	Wb ($V \cdot s$)
Magnetic flux density	Tesla	T (Wb/m^2)
Magnetic field strength	H	A/m
Inductance	Henry	H (Wb/A)
Magnetic moment	m	m ($A \cdot m^2$)
Magnetization	M	M (A/m)

Magnetic Units - selection

Quantity/name	Symbol	Gaussian & cgs emu	Conversion factor, C	SI & rationalized MKS
Magnetic flux density (magnetic induction)[a]	B	Gauss (G)	10^{-4}	Tesla (T), Wb/m^2
Magnetic flux	Φ	Maxwell (Mx), $G \cdot cm^2$	10^{-8}	Webber (Wb), $T \cdot m^2 = V \cdot s$
Magnetic polarization (intensity of magnetization)	J	emu/cm^3	$4\pi \cdot 10^{-4}$	T, Wb/m^2
Magnetic field strength[a]	H	Oersted (Oe)	$10^3/4\pi$	A/m
Volume magnetization	M	emu/cm^3	10^3	A/m
Mass magnetization	M, σ	emu/g	1 $4\pi \cdot 10^{-7}$	$A \cdot m^2/kg$ $Wb \cdot m/kg$
Magnetic susceptibility	χ	dimensionless	4π	dimensionless
Magnetic permeability	μ	dimensionless	$4\pi \cdot 10^{-7}$	H/m, $Wb/(A \cdot m)$
Demagnetization factor	N	dimensionless	$1/4\pi$	dimensionless

[a]In CGS de defining relation is $B = H + 4\pi \cdot M$ whereas in SI the relation is $B = \mu_0(H+M) = \mu_0 \cdot H + J$ where $J = \mu_0 M$ is *magnetic polarization*.

Bibliography

[1] Marius Volmer, Nanostructuri magnetice – Obținere, proprietăți, aplicații, Editura Universității Transilvania din Braşov, 2008, ISBN 978-973-598-248-5;

[2] Jacob Fraden, Handbook of modern sensors – Physics, Design and Applications, Springer, 2016, ISBN: 978-3-319-19303-8; https://doi.org/10.1007/978-3-319-19303-8

[3] Data Acquisition Handbook; A Reference For DAQ and Analog & Digital Signal Conditioning, 2004-2012 by Measurement Computing Corporation; http://www.mccdaq.com/pdfs/anpdf/data-acquisition-handbook.pdf

[4] Simulmag, http://math.nist.gov/oommf/contrib/simulmag/

[5] OOMMF, https://math.nist.gov/oommf/

[6] https://www.sensitec.com/service-support/download

[7]https://www.sensitec.com/fileadmin/sensitec/Service_and_Support/Downloads/Catalogue/Sensitec_Katalog2015_Web_LZen.pdf

[8] https://www.nve.com/analogSensors

[9] https://www.nve.com/spec/calculators#tabs-Current-Sensing

[10] https://www.nve.com/EvaluationKits

[11] https://labjack.com/

[12] Mușuroi, C., Oproiu, M., Volmer, M., Neamtu, J., Avram, M., & Helerea, E., Low Field Optimization of a Non-Contacting High-Sensitivity GMR-Based DC/AC Current Sensor. Sensors, 21(7), 2564 (2021),, https://doi.org/10.3390/s21072564

[13] https://wokwi.com/

[14] https://www.instructables.com

[15] Reynolds, S., Brinza, M., Benkhedir, M.L., Adriaenssens, G.J. (2017). Photoconductivity in Materials Research. In: Kasap, S., Capper, P. (eds) Springer Handbook of Electronic and Photonic Materials. Springer Handbooks. Springer, Cham. https://doi.org/10.1007/978-3-319-48933-9_7

[16] https://sourceforge.net/projects/scidavis/

[17] https://electronicscoach.com/photodiode.html

[18] https://www.electricaltechnology.org/2022/01/difference-between-photodiode-phototransistor.html

[19] https://web.archive.org/web/20141113175955/http://www.pacer.co.uk/Assets/Pacer/User/Photodiodes.pdf